

# A finite strain fibre-reinforced viscoelasto-viscoplastic model of plant cell wall growth

R. Huang<sup>1</sup> , A. A. Becker<sup>2</sup>, I. A. Jones<sup>2</sup>

<sup>1</sup> School of Mathematics and Statistics, University of Glasgow, Glasgow G12 8QW, UK

<sup>2</sup> Department of Mechanical, Materials and Manufacturing Engineering, University of Nottingham, Nottingham, NG7 2RD, UK

## Abstract

A finite strain fibre-reinforced viscoelasto-viscoplastic model implemented in a Finite Element (FE) analysis is presented to study the expansive growth of plant cell walls. Three components of the deformation of growing cell wall, i.e. elasticity, viscoelasticity, and viscoplasticity-like growth, are modelled within a consistent framework aiming to present an integrative growth model. The two aspects of growth, turgor-driven creep and new material deposition, and the interplay between them are considered by presenting a yield function, flow rule, and hardening law. A fibre-reinforcement formulation is used to account for the role of cellulose microfibrils in the anisotropic growth. Mechanisms in *in vivo* growth are taken into account to represent the corresponding biology-controlled behaviour of a cell wall. A viscoelastic formulation is proposed to capture the viscoelastic response in the cell wall. The proposed constitutive model provides a unique framework for modelling both the *in vivo* growth of cell wall dominated by viscoplasticity-like behaviour and *in vitro* deformation dominated by elastic or viscoelastic responses. A numerical scheme is devised and FE case studies are reported and compared with experimental data.

**Keywords** biological material · constitutive behaviour · fibre-reinforced composite material · viscoplastic material · finite strain · Finite Element analysis · cell wall growth

**Corresponding author:** Dr. R. Huang, Email: ruoyu.huang@glasgow.ac.uk

# 1 Introduction

The understanding of cell wall expansion is a fundamental issue in plant biology (see, e.g. Refregier *et al.* [1]). It is widely accepted that plant cell walls are considered to be composites in which cellulose microfibrils are embedded into an amorphous matrix composed of hemicellulose, pectins and proteins. The composite must satisfy two conflicting requirements. It must be strong enough to resist the mechanical stress (which may exceed  $10^8 \text{ Nm}^{-2}$  (100 MPa)) generated by the cell turgor pressure and at the same time it must be sufficiently compliant to permit irreversible wall expansion. The cell wall accommodates these requirements through its composite structure, having stiff microfibrils with high mechanical strength embedded in a viscoplastic amorphous matrix that moves in a controlled fashion [2].

Fig. 1 shows a schematic structure of a full anisotropic cell wall. The cellulose molecules form semi-crystalline microfibrils, several nm in width and many  $\mu\text{m}$  long, which may be cross-linked by hemicelluloses molecules [3]. Microfibrils have a tensile strength similar to that of steel, and are relatively inert and inextensible in growth [4][5]. The matrix consists of cellulose-binding polysaccharides (hemicelluloses) that form a load-bearing network with cellulose microfibrils, as well as hydrophilic pectic polysaccharides and structural proteins elaborated around the microfibril scaffold [5]. Neighbouring microfibrils tend to be approximately parallel, giving the cell wall a mat-like appearance and a distinct structural anisotropy broadly similar in structure to a multi-layered laminate [6]. Thus the cell wall can be modelled as a fully anisotropic composite [7] in which continuous microfibrils are aligned preferentially in one direction inside a representative element (see Fig. 1).

In contrast to cellulose microfibrils which mainly play a load-bearing role, the cross-links are related with cell wall loosening which is the most crucial step in cell wall growth and the key to connect expansive growth with plasticity material models. The wall loosening refers to the rearrangement of load-bearing cross-links which must occur in order to relax the wall stress and to allow polymer slippage as water is taken in and the wall expands irreversibly [8]. In this interpretation, wall loosening is analogous to, and is referred to in the biological literature as (plastic) yielding. The irreversible expansion is therefore referred to as plastic deformation. Although the molecular details of wall loosening are largely unknown, there is convincing evidence that cells produce some kind of a wall-loosening factor that mediates a metabolically controlled chemo-rheological process facilitating the plastic deformation of the cell walls under the tensile force produced by turgor pressure [9]. The idea of a wall loosening enzyme, e.g. enzymes which can break and transfer cross-links, is prevailing [8]. This idea is analogous to the concept of crystal slip in plasticity, allowing the implementation of an equivalent plasticity model of cell wall growth. However, it should be borne in mind that loosening is regulated by chemical entities, e.g. expansins, and the turgor pressure is actively maintained by the cell itself, so that stress is a *passive* driving force for expansion in the sense that chemical regulation actively controls the growth. The role of expansins in cell wall loosening is reviewed by Cosgrove [10][11][12] and by Choi *et al.* [13].

However, it is noted that the turgor-driven expansive growth of the cell surface by turgor pressure cannot proceed without the addition of new wall material, because the cell wall would quickly become thinner and eventually rupture [7]. Wall loosening must therefore be accompanied by wall reinforcement in order to maintain the strength of the expansion. This requirement is generally satisfied by the synthesis of cellulose and other polysaccharides and their apposition to the inner surface of the wall (new material deposition). However, this is not just a process to maintain the geometry, e.g. wall thickness, as reported extensively in the literature [7][14][15]. More importantly, the dynamic process of *in vivo* cell expansive growth depends on a delicate mechanical regulation to maintain the balance of wall-loosening and wall-stiffening processes [9]. A proper mechanical model should adequately represent these constitutive responses which indicate an intrinsic role of mechanics

in cell wall expansive growth. Therefore, how the expansive growth integrates with wall deposition to generate a growth-sustaining activity is the key issue of mechanical modelling of *in vivo* cell growth [16]. Mixture theory (e.g.[17]) may be one of natural candidates to account for the deposition but is outside the scope of the present study.

In addition to growth, the other time-dependent feature, i.e. viscoelasticity, which is the collection of relaxation, creep, and hysteresis [18], was widely observed in mechanical responses of the cell walls [8][19][20]. However, because both are time-dependent, it is not always easy to distinguish viscoelastic response from growth. For example, whether *in vitro* growth is a viscoplastic or viscoelastic response is still an open question which provides a typical case to illustrate the complexity the time-dependent behaviours of the cell wall [6][9]. In general, the mechanical response of the growing cell wall may contain both the viscoelastic and viscoplastic components. Based on their experimental observation, Proseus and Boyer [16] diagrammatically summarised the general behaviour of the growing cell wall in the loading and unloading processes. As shown in Fig. 2, turgor pressure can be raised or lowered by injecting or removing the cell solution. When the turgor pressure decreases from its normal level, the cell wall has an instant elastic response and the growth rate also decreases from its normal value. By contrast, when turgor pressure increases and returns to its normal level, the cell wall experiences an instant elastic response at first and then a gradual transition until the growth rate returns back to its normal value. This diagrammatical conclusion indicates one of the crucial characteristics of a cell wall, i.e. it has different viscoelastic behaviours in the loading and unloading processes, which is a typical mechanical response of cell wall to the change of turgor pressure reported in extensive experimental observations [8]. In order to model such a viscoelastic response of the growing cell wall, viscoelastic and viscoplastic behaviours need to be integrated in a united model. To the authors' knowledge, there is no reported model that can model the whole behaviour in Fig. 2 combining elastic, viscoelastic and viscoplastic responses.

Lockhart [21][22] summarized a wide range of experimental data on wall extensibility in a formula that was readily comprehensive and became established as the well-known 'Lockhart equation':

$$r_g = \Phi(P - Y) \quad (1)$$

where  $r_g$  is the growth strain rate which is either nonzero for  $P > Y$  or zero for  $P \leq Y$ ,  $\Phi$  is the extensibility of the cell wall,  $P$  is the turgor pressure and  $Y$  is the yield threshold, i.e. the minimum pressure required for growth [23]. Lockhart equation and its other modified expressions (see, e.g. [9][24-28]) shed light on the viscoplastic behavior of cell wall growth and has been extensively used in biological research.

Different tensor-based models have been suggested to develop and improve the Lockhart equation. Pietruszka [29] presented a tensor format of the original Lockhart equation. Veytsman and Cosgrove [30] reported a thermodynamic modelling of polymer networks. Another method is to directly apply (elasto-visco) plasticity theory taking the Lockhart equation as its consistent volumetric or uniaxial format. Boudaoud [31] investigated the growth of isolated walled cells which is driven by fluid pressure and is similar to a perfectly-plastic deformation of shells containing a liquid. Dumais *et al.* [7] developed an anisotropic viscoplastic thin shell model of cell walls which was a first attempt at integrating mechanical deformation driven by turgor pressure and new material deposition.

In contrast to the Lockhart equation and those models based on the concept that the unique characteristics of cell wall growth lie in the yielding of the wall matrix, the other class of models focused on the concept that cellulose microfibrils are the most pronounced structural units of the cell wall and play a role as mechanical constraints which regulate the anisotropic growth [32][33]. Hettiaratchi and O'Callaghan [34] proposed a fibre-reinforced elastic model of cell walls assuming that the cell wall matrix can be characterised either by neo-Hookean or Mooney-Rivlin material models and the microfibrils were treated as thin inextensible cords. By using the analogy between plant cell and cardiac tissue, Chaplain [35] suggested that the strain energy of plant cell walls has a

similar form to that of a cardiac tissue in which microfibrils were treated as extensible. Dyson and Jensen [36] suggested a fiber-reinforced viscous fluid model which considered the time-dependent behaviour of cell walls. Dyson *et al.* [37] then examined the influence of enzyme action upon the weakening of the cross-links. Geitmann [38] reviewed a number of approaches to the modelling of cell walls to reflect the mechanisms that take place during their expansion. Geitmann [39] also explored the mechanisms by which plant cells expand, with particular reference to the mechanics of tip growth and its dependence upon the mechanical properties of the cell wall. Kha *et al.* [40] describe a program for generating finite element models of cellulose/hemicelluloses networks in order to predict their properties, explicitly modelling individual microfibrils and cross-links.

In addition, modelling cell wall growth by elasticity theory without explicit formulation of fibre-reinforcement provides useful insight into the morphogenesis of cell wall. The tip growth of filamentary actinomycetes is investigated by Goriely and Tabor [41] within the framework of large deformation membrane theory in which the cell wall is represented as a growing elastic membrane with geometry-dependent elastic properties filled with an incompressible viscous fluid. Bernal *et al.* [42] showed that tubular rubber balloons offer a useful physical model of tip growth morphogenesis of plant, fungal, and bacterial cells. It is noted that for its simplicity, the elastic model is widely used in finite element modelling of plant growth [43][44]. A comprehensive literature review on elastic modelling of plant cell wall was reported by Bruce [32].

From the point of view of integrative biology, the various existing models in literature gave insight into some aspects of cell wall growth, e.g. elasticity, viscosity, plasticity and deposition of material, but a constitutive model which integrates the different aspects together by accommodating different hypotheses in a consistent framework has not been reported [45]. However, the complex nature of the cell wall growth and existence of competing modelling methodologies for the growth of soft tissue, e.g. single phase modelling [39][46-48], mixture theory [49] and modelling based on the concept of natural configuration [50], imply that there is no single approach which is superior to others in all aspects of modelling. Therefore, the present study focuses on single phase (solid) modelling and tries to present a general framework for modelling cell wall growth based on solid mechanics.

In order to present a platform for establishing and developing the integrative model of cell wall growth, a fibre-reinforced elasto-viscoplastic model of the cell wall growth was discussed in our previous work based on direct analogy between the cell wall growth and metal plasticity [51]. The essence of growth as a viscoplastic response was emphasised and the mechanisms and hypotheses of growth were formulated in the framework of viscoplasticity. Consistent with the well-known Lockhart's model, the model proposed by Huang *et al.* [51] could capture the important characteristics of the growing cell wall, which had not been reported, to be modelled by any other existing single model. However, since viscoelasticity was not been taken into account, the verification of this cell wall model against experimental observations is limited to case studies with negligible viscoelasticity. As viscoelasticity is a universal response in natural biomaterials [18] and cannot be ignored in many experimental observations on cell wall growth [8][16], an extended constitutive model with viscoelastic response is proposed in the present work and is expected to substantially improve the modelling of the cell wall growth. The typical mechanical response shown in Fig. 2 can be modelled in a single 3D model by using the present extended model. Moreover, the present constitutive model can be applied straightforwardly to both the *in vivo* growth of cell wall dominated by viscoplastic behaviour and *in vitro* deformation dominated by elastic or viscoelastic responses. In this way, the model can be helpful for understanding and clarifying the complexity of cell wall behaviours, e.g. whether *in vitro* growth is a viscoplastic or a viscoelastic response, from the point of view of integrative modelling.

In the present work a finite strain fibre-reinforced viscoelasto-viscoplastic model, which is started from general thermodynamic principles rather than from the analogy between the cell wall growth and

metal plasticity is proposed to cover a wider range of experimental observations. As an integrative model established from fundamental principles of mechanics/thermodynamics, it can account for the complexity of the cell wall growth in a rational way.

The present phenomenological model is outlined as follows. Firstly, kinematic theory is discussed to characterise the different components of deformation, and the corresponding configurations are defined. Especially, extra configuration is introduced to model the different viscoelastic responses in the loading and unloading processes. Secondly, the Clausius-Duhem inequality is used to establish the framework of the constitutive modelling and to introduce an appropriate free energy function. Thirdly, the viscoelastic response is modelled based on the general framework suggested by Simo and Hughes [52]. Fourthly, the growth is treated as an anisotropic viscoplastic response and is formulated within the general framework suggested by Moran *et al.* [53] and Belytschko *et al.* [54]. Finally, based on the integrative constitutive model, a finite element (FE) scheme is suggested and implemented in the ABAQUS<sup>®</sup> FE computer code to model the interplay among expansive growth, turgor pressure and temperature.

## 2 Kinematics of the model

### 2.1 Basic kinematics

At a certain initial time, the cell wall is represented as a continuum composite having a reference configuration,  $B_0$ , with material points labelled by  $\mathbf{X} \in B_0$ . At any current time,  $t \in [0, +\infty)$ , a mapping  $\varphi: B_0 \rightarrow B_t$  is a deformation which maps the reference configuration  $B_0$  onto the current configuration  $B_t$  embedded into Euclidean space  $R^3$ . The current position of a material point  $\mathbf{X}$  is written as  $\mathbf{x} = \varphi(\mathbf{X}, t) \in B_t \subset R^3$ . The deformation gradient is defined as  $\mathbf{F}(\mathbf{X}, t) = \partial\varphi/\partial\mathbf{X}$  with its Jacobian denoted as  $J = \det \mathbf{F} > 0$ . In addition, the right and left Cauchy-Green tensors are defined respectively as [55]

$$\mathbf{C} = \mathbf{F}^T \mathbf{F}, \quad \mathbf{b} = \mathbf{F} \mathbf{F}^T. \quad (2)$$

To be consistent with the full anisotropic cell wall shown schematically in Fig. 1, it is assumed that there is a single family of microfibrils inside a representative element of cell wall. Therefore, resorting to the terminology of the Cosserat continuum [55], the local (averaged) kinematics of microfibrils can be represented by a deformation of an extensible *director* attached to a representative material point. In the reference configuration, the director is represented by a unit vector  $\mathbf{a}_0(\mathbf{X}) \in \mathcal{S}^2$ , where  $\mathcal{S}^2$  is the unit sphere in  $R^3$ , and is used to model vectors that are free to point in any direction [55]. By using the perfect matrix-fibre bonding assumption [56], at time  $t$  the director is mapped into its current configuration

$$\mathbf{a}(\mathbf{X}, t) = \mathbf{F}(\mathbf{X}, t) \mathbf{a}_0(\mathbf{X}) \in R^3. \quad (3)$$

Thus the deformation gradient  $\mathbf{F}$  suffices to define both the spatial direction

$$\tilde{\mathbf{a}} = \mathbf{a} / \sqrt{\lambda_a}, \quad \tilde{\mathbf{a}} \cdot \tilde{\mathbf{a}} = 1 \quad (4)$$

and the extension (stretch) of the director

$$\sqrt{\lambda_a} = \sqrt{\mathbf{C} : \mathbf{A}_0} = \sqrt{\text{tr} \mathbf{A}} \quad (5)$$

where  $\mathbf{A}_0 = \mathbf{a}_0 \otimes \mathbf{a}_0$  and  $\mathbf{A} = \mathbf{a} \otimes \mathbf{a}$  with Cartesian components  $(\mathbf{A}_0)_{IJ} = a_{0I}a_{0J}$  and  $(\mathbf{A})_{ij} = a_i a_j$  respectively are defined to be structural tensors of order two, symbols ‘ $\cdot$ ’ and ‘ $\otimes$ ’ denote the double contraction of tensors and the dyadic product respectively, and the symbol ‘tr’ denotes the trace of a tensor.

Therefore, the basic kinematics of model is described as the deformation  $\varphi: B_0 \rightarrow B_t$  mapping the pair of variables  $(\mathbf{X}, \mathbf{a}_0) \in B_0 \times S^2$  onto  $(\mathbf{x}, \mathbf{a}) \in B_t \times R^3$ .

## 2.2 Multiplicative decompositions of the deformation gradients

Skalak, Fung, and co-workers [57-60] pointed out that if the growth strains of each element of an originally unloaded and stress-free body are geometrically compatible, then the body remains *stress-free* after the growth occurs. If the growth strains are incompatible, however, internal (residual) stresses are generated. Combining and extending the ideas of Skalak, Fung, and co-workers. Rodriguez *et al.* [61] suggested a kinematical *multiplicative decomposition* of the total deformation gradient,  $\mathbf{F}$ , into the *mechanical* part and the *growth* part as  $\mathbf{F} = \mathbf{F}^e \mathbf{F}^g$ . Here, tensor  $\mathbf{F}^g$  is the deformation solely due to the growth of material, which is not constrained by the surroundings and leaves the material in a zero-stress state. Tensor  $\mathbf{F}^e$  is the accompanying elastic deformation that ensures the compatibility of the total deformation. This decomposition is analogous to the counterpart in phenomenological plasticity suggested by Lee and others [62].

In order to account for the viscoelastic response of the cell wall, the Rodriguez’s formulation is modified as

$$\mathbf{F} = \mathbf{F}^{ve} \mathbf{F}^g \quad (6)$$

in which  $\mathbf{F}^{ve}$  is viscoelastic part of the deformation gradient. The whole viscoelastic response can be represented by the deformation gradient  $\mathbf{F}^{ve}$  and appropriate stress-like internal variables (e.g.  $\tilde{\mathbf{Q}}$  and  $\hat{\mathbf{Q}}$  in eqn.(17)). A multiplicative decomposition of viscoelastic deformation gradient for representing the different viscoelastic responses in loading and unloading processes is suggested as follows

$$\mathbf{F}^{ve} = \tilde{\mathbf{F}} \hat{\mathbf{F}} \quad (7)$$

where  $\tilde{\mathbf{F}}$  and  $\hat{\mathbf{F}}$  are two tensors that represent the history of viscoelastic responses to loading and unloading, respectively.

Following plasticity theory, the decomposition in eqn.(6) leads to the notion of a (local) stress-free *intermediate configuration*,  $\bar{B}_t$ , which consists of a collection of plastically deformed neighbourhoods defined by a pull-back  $\mathbf{F}^{ve-1}$  from  $B_t$  onto  $\bar{B}_t$  (see Fig. 3).  $\mathbf{F}^{ve-1}$  as the local deformation releases the residual stress due to incompatibility of unconstrained growth from each neighbourhood on  $B_t$ .

In a similar way, an extra intermediate configuration,  $\tilde{B}_t$ , corresponding to the decomposition in eqn.(7) is defined here by a pull-back  $\tilde{\mathbf{F}}^{-1}$  from  $B_t$  onto  $\tilde{B}_t$  as shown in Fig. 3.  $\tilde{B}_t$  represents the history record of the viscoelastic response to unloading/loading, or more precisely the record of the accumulation of all instant viscoelastic response to loadings, noting that  $\tilde{B}_t$  is not the Maxwell body used in some viscoelasticity literature (see e.g. [63]). The Maxwell body should evolve with respect to

time when away from thermodynamic equilibrium and coincide with the current configuration  $B_t$  at thermodynamic equilibrium. By contrast,  $\tilde{B}_t$  as an internal variable is changed by loading/unloading history only. The Maxwell body is not explicitly mentioned in the present work since its role is taken over by the stress-like internal variables (see the evolution of stress-like viscoelastic internal variables  $\tilde{Q}$  and  $\hat{Q}$  in eqns.(36)(37) and their thermodynamic-equilibrium state (46)(47)).

Using standard conventions in continuum mechanics, the viscoelastic right and left Cauchy-Green tensors are defined respectively as

$$\bar{\mathbf{C}} = \mathbf{F}^{veT} \mathbf{F}^{ve}, \quad \bar{\mathbf{b}} = \mathbf{F}^{ve} \mathbf{F}^{veT}. \quad (8)$$

Let  $\mathbf{g}$  be the metric tensor on the current configuration  $B_t$ . As  $B_t$  is embedded into Euclidean space  $R^3$ , without loss in generality, let  $\mathbf{g} = \mathbf{I}$  where  $\mathbf{I}$  denotes the symmetric unit tensor with components  $\delta_{ij}$  (where  $\delta_{ij}$  is the Kronecker delta) in a Cartesian reference system. Thus the viscoelastic right Cauchy-Green tensor  $\bar{\mathbf{C}}$ , which is interpreted as a tensor defined by pulling back the metric tensor  $\mathbf{g}$  from  $B_t$  onto  $\bar{B}_t$ , is the metric tensor on  $\bar{B}_t$ . Similarly, the right Cauchy-Green tensor  $\tilde{\mathbf{C}} = \tilde{\mathbf{F}}^T \tilde{\mathbf{F}}$  is the metric tensor on  $\tilde{B}_t$ .

Let  $\mathbf{L} = \partial \dot{\mathbf{x}} / \partial \mathbf{x} = \dot{\mathbf{F}} \mathbf{F}^{-1}$  be the spatial velocity gradient, where the symbol of superimposed dot denotes the material time derivative. By using the decomposition (6), the decomposition of  $\mathbf{L}$  is obtained as follows

$$\mathbf{L} = \dot{\mathbf{F}}^{ve} \mathbf{F}^{ve-1} + \mathbf{F}^{ve} \dot{\mathbf{F}}^g \mathbf{F}^{g-1} \mathbf{F}^{ve-1} = \mathbf{L}^{ve} + \mathbf{L}^g. \quad (9)$$

Similarly the decomposition of  $\mathbf{L}^{ve}$  is defined according to eqn.(7) as

$$\mathbf{L}^{ve} = \dot{\tilde{\mathbf{F}}} \tilde{\mathbf{F}}^{-1} + \tilde{\mathbf{F}} \hat{\dot{\mathbf{F}}} \tilde{\mathbf{F}}^{-1} \tilde{\mathbf{F}}^{-1} = \tilde{\mathbf{L}} + \hat{\mathbf{L}}. \quad (10)$$

The definition of the configuration  $\tilde{B}_t$  is set to be based on a kinematic update criterion, as follows

$$\begin{cases} \text{if } \text{tr} \mathbf{L}^{ve} < 0 & \tilde{\mathbf{L}} = \mathbf{0}, \quad \hat{\mathbf{L}} = \mathbf{L}^{ve} \\ \text{if } \text{tr} \mathbf{L}^{ve} \geq 0 & \tilde{\mathbf{L}} = \mathbf{L}^{ve}, \quad \hat{\mathbf{L}} = \mathbf{0} \end{cases}. \quad (11)$$

Therefore, eqn. (11) defines  $\tilde{\mathbf{F}}$  and  $\hat{\mathbf{F}}$  as the history of viscoelastic responses to loading and unloading, respectively. The symmetric parts of  $\mathbf{L}^{ve}$ ,  $\mathbf{L}^g$ ,  $\tilde{\mathbf{L}}$  and  $\hat{\mathbf{L}}$  are denoted respectively as

$$\mathbf{D}^{ve} = (\mathbf{L}^{ve} + \mathbf{L}^{veT}) / 2, \quad \mathbf{D}^g = (\mathbf{L}^g + \mathbf{L}^{gT}) / 2. \quad (12)$$

$$\tilde{\mathbf{D}} = (\tilde{\mathbf{L}} + \tilde{\mathbf{L}}^T) / 2, \quad \hat{\mathbf{D}} = (\hat{\mathbf{L}} + \hat{\mathbf{L}}^T) / 2. \quad (13)$$

Eqns. (12) and (13) lead to the decomposition of the rate of deformation tensors,  $\mathbf{D} = \mathbf{D}^{ve} + \mathbf{D}^g$  and  $\mathbf{D}^{ve} = \tilde{\mathbf{D}} + \hat{\mathbf{D}}$ , on  $B_t$ .

Mapping  $\mathbf{L}^{ve}$  and  $\mathbf{L}^g$  back to the intermediate configuration  $\bar{B}_t$ , we obtain the viscoelastic and growth parts of the velocity gradient on  $\bar{B}_t$  respectively as

$$\bar{\mathbf{L}}^{ve} = \mathbf{F}^{ve-1} \dot{\mathbf{F}}^{ve}, \quad \bar{\mathbf{L}}^g = \dot{\mathbf{F}}^g \mathbf{F}^{g-1}. \quad (14)$$

The viscoelastic and growth rates of deformation tensors on  $B_t^-$ , denoted as  $\bar{D}^{ve}$  and  $\bar{D}^g$ , are defined by the symmetric parts of  $\bar{L}^{ve}$  and  $\bar{L}^g$  respectively as

$$\bar{D}^{ve} = \text{sym} \bar{L}^{ve} \square (\bar{C} \bar{L}^{ve} + \bar{L}^{veT} \bar{C}) / 2, \quad \bar{D}^g = \text{sym} \bar{L}^g \square (\bar{C} \bar{L}^g + \bar{L}^{gT} \bar{C}) / 2. \quad (15)$$

### 3 Thermodynamic aspects

In essence, the growing cell wall is a complex open system with thermodynamic variables characterising mass transport between the wall and its environment. Considering the essential difference between the open system and the closed system, a brief discussion on the thermodynamic aspects of modelling is necessary for justifying the application of solid mechanics, which conventionally accounts for closed system only, to growth. Moreover, thermodynamics is a helpful starting point to unify the complex behaviours of growth in an integrative platform.

Because there is no experimental evidence indicating that the change of wall material density is essential in wall growth, it is assumed in the present work that the change of density of cell wall is solely resulted from elastic deformation. Therefore, growth law involving constitutive law of change of material density [47][56] is not considered here. Based on the growth mechanisms, the cell wall growth can be defined as a system containing the turgor-driven isochoric (volume-invariant) expansion and volumetric growth. The former is a typical deformation in a closed system, the latter, however, is behaviour in an open system.

The volumetric growth of cell wall is a process of insertion, deposition and transport of new material from the wall environment into the wall composite. However, In order to capture the features of growth by a model using a reasonable complexity and to implement the model straightforwardly into a commercial finite element software package, we assume that there is no mass diffusive effect and the new wall material is produced by a smooth volumetric source of mass. The assumption is consistent with the model for dealing with the mass generation and removal during growth of soft tissue proposed by Humphrey and Rajagopal [50][64] as they argued that, although the *mechanism* by which volumetric growth takes place is ignored, the *result* of volumetric growth is captured.

By using the assumption of no mass diffusive effect and a volumetric source of mass, the unconventional quantities related with mass growth in an open system (e.g. irreversible momentum flux) are either set to vanish or are absorbed into a set of thermodynamic variables of a closed mechanical system (see the first order theory of volumetric growth [46] or the open system theory retaining the form of closed system theory [47]). Therefore, in the present study the expression of the second law of the thermodynamics of the cell wall growth is in the same form as that of a closed system.

The Clausius-Duhem inequality of the isothermal model of cell wall growth is [65]

$$\mathbf{D} = \boldsymbol{\tau} : \mathbf{D} - \dot{\psi} \geq 0 \quad (16)$$

where  $\mathbf{D}$  is the dissipation function,  $\boldsymbol{\tau}$  is Kirchhoff stress,  $\psi$  is Helmholtz's free energy which is assumed to depend on a set of thermodynamic variables, i.e. the right Cauchy-Green tensor  $\bar{C}$ , stress-like viscoelastic internal variables  $\tilde{\mathbf{Q}}$  and  $\hat{\mathbf{Q}}$  on  $B_t^-$  corresponding to  $\tilde{\mathbf{F}}$  and  $\hat{\mathbf{F}}$  respectively, and plastic hardening parameter  $\alpha$ . Thus we have

$$\dot{\psi}(\bar{C}, \tilde{\mathbf{Q}}, \hat{\mathbf{Q}}, \alpha) = 2 \frac{\partial \psi}{\partial \bar{C}} : \bar{D}^{ve} + \frac{\partial \psi}{\partial \tilde{\mathbf{Q}}} : \dot{\tilde{\mathbf{Q}}} + \frac{\partial \psi}{\partial \hat{\mathbf{Q}}} : \dot{\hat{\mathbf{Q}}} + \frac{\partial \psi}{\partial \alpha} \dot{\alpha}. \quad (17)$$

Substituting eqn. (17) into inequality (16) yields

$$\bar{\mathbf{S}} = 2 \frac{\partial \psi}{\partial \bar{\mathbf{C}}} \quad (18)$$

and

$$\mathbf{D} = \underbrace{\bar{\mathbf{S}} : \bar{\mathbf{D}}^g - q \dot{\alpha}}_{\mathbf{D}_g} - \underbrace{\frac{\partial \psi}{\partial \tilde{\mathbf{Q}}} : \dot{\tilde{\mathbf{Q}}} - \frac{\partial \psi}{\partial \hat{\mathbf{Q}}} : \dot{\hat{\mathbf{Q}}}}_{\mathbf{D}_{ve}} \geq 0 \quad (19)$$

where  $\bar{\mathbf{S}}$  is the second Piola-Kirchhoff stress on  $\bar{\mathbf{B}}_t$ , the stress-like variable,  $q$ , is defined as  $q = \partial \psi / \partial \alpha$ . Inequality (19) is a constraint on the constitutive model. It is noted that the constraint (19) can be satisfied if the set of stronger constraints (20) is satisfied as follows

$$\mathbf{D}_g = \bar{\mathbf{S}} : \bar{\mathbf{D}}^g - q \dot{\alpha} \geq 0, \quad \mathbf{D}_{ve} = -\frac{\partial \psi}{\partial \tilde{\mathbf{Q}}} : \dot{\tilde{\mathbf{Q}}} - \frac{\partial \psi}{\partial \hat{\mathbf{Q}}} : \dot{\hat{\mathbf{Q}}} \geq 0 \quad (20)$$

where  $\mathbf{D}_g$  and  $\mathbf{D}_{ve}$  represent the growth and viscoelastic parts of dissipation, respectively. The present constitutive modelling would aim to satisfy the constraints (20). Consequently, the growth and viscoelastic parts of dissipation can be discussed separately and constraint (19) can be satisfied.

In order to be consistent with the viscoelastic theory proposed by Simo and Hughes [52], an expression of free energy is suggested to have the following form

$$\psi(\bar{\mathbf{C}}, \tilde{\mathbf{Q}}, \hat{\mathbf{Q}}, \alpha) = \Psi(\bar{\mathbf{C}}) + H(\alpha) - \bar{J}^{-2/3} \tilde{\mathbf{C}} : \tilde{\mathbf{Q}} - \bar{J}^{-2/3} \bar{\mathbf{C}} : \hat{\mathbf{Q}} + \tilde{\Phi}(\tilde{\mathbf{Q}}) + \hat{\Phi}(\hat{\mathbf{Q}}) \quad (21)$$

where a hardening potential is assumed as  $H = \frac{1}{2} K \alpha^2$ , the Jacobian on  $\bar{\mathbf{B}}_t$  is defined as  $\bar{J} = \det \mathbf{F}^{ve}$ , the tensor  $\tilde{\mathbf{Q}}$  is obtained by pushing  $\hat{\mathbf{Q}}$  forward from  $\bar{\mathbf{B}}_t$  onto  $\tilde{\mathbf{B}}_t$  as  $\tilde{\mathbf{Q}} = \hat{\mathbf{F}} \hat{\mathbf{Q}} \hat{\mathbf{F}}^T$ , and  $\tilde{\Phi}$  and  $\hat{\Phi}$  are two functions to be defined in the next section (see eqn.(49)).

Substituting eqn.(21) into eqn. (18) and inequalities (20) and using eqn.(A29) yield the expressions of stress  $\bar{\mathbf{S}}$  and viscoelastic dissipation as follows

$$\bar{\mathbf{S}} = \bar{\mathbf{S}}^e - \bar{J}^{-2/3} \text{DEV}[\tilde{\mathbf{Q}} + \hat{\mathbf{Q}}], \quad (22)$$

and

$$\mathbf{D}_{ve} = \left( \bar{J}^{-2/3} \tilde{\mathbf{C}} - \frac{\partial \tilde{\Phi}}{\partial \tilde{\mathbf{Q}}} \right) : \dot{\tilde{\mathbf{Q}}} + \left( \bar{J}^{-2/3} \bar{\mathbf{C}} - \frac{\partial \hat{\Phi}}{\partial \hat{\mathbf{Q}}} \right) : \dot{\hat{\mathbf{Q}}} \geq 0 \quad (23)$$

where  $\bar{\mathbf{S}}^e = 2 \partial \Psi / \partial \bar{\mathbf{C}}$  is the hyperelastic component of stress  $\bar{\mathbf{S}}$ , deviatoric operator  $\text{DEV}[\square] = (\square) - \frac{1}{3} \text{Tr}(\square) \bar{\mathbf{C}}^{-1}$  on  $\bar{\mathbf{B}}_t$  is the counterpart of  $\text{dev}[\square] = (\square) - \frac{1}{3} \text{tr}(\square) \mathbf{I}$  on  $\mathbf{B}_t$ . Whereby the function  $\text{Tr}(\square)$  is defined on  $\bar{\mathbf{B}}_t$  as  $\text{Tr}(\square) = \bar{\mathbf{C}} : (\square)$  which is the counterpart of  $\text{tr}(\square) = \mathbf{I} : (\square)$  on  $\mathbf{B}_t$ . The stress-like variable,  $q$ , in eqn.(19) is expressed as  $q = K \alpha$ .

## 4 Viscoelastic response

Proseus and Boyer [16] suggested that there are two kinds of intermolecular bonds in a cell wall matrix; the strong bonds which are responsible for growth, and the weak bonds which are attributed to elastic extension. This suggestion leads to the assumption that the viscoelastic response is unaffected by plastic flow which provides the physical basis for the multiplicative decomposition (6) and the viscoelastic formulation on the intermediate configuration.

The viscoelastic response of the cell wall is defined in eqn.(22) with contributions from the hyperelastic component  $\bar{\mathbf{S}}^e$  and internal variables  $\tilde{\mathbf{Q}}$  and  $\hat{\mathbf{Q}}$ . In the present study, on the one hand, the strain invariants theory of fibre-reinforced hyperelastic model suggested by Gasser *et al.* [56] is adopted for obtaining a specified function  $\Psi$  in eqn.(21) to calculate  $\bar{\mathbf{S}}^e$ . On the other hand, the evolution equations of the internal variables,  $\tilde{\mathbf{Q}}$  and  $\hat{\mathbf{Q}}$ , are proposed. With  $\bar{\mathbf{S}}^e$ ,  $\tilde{\mathbf{Q}}$  and  $\hat{\mathbf{Q}}$  obtained, the second Piola-Kirchhoff stress  $\bar{\mathbf{S}}$  is calculated by eqn.(22), and the viscoelastic tangent modulus  $\bar{\mathbf{C}}$  on the intermediate configuration can be calculated as follows

$$\bar{\mathbf{C}} = 2 \frac{\partial \bar{\mathbf{S}}}{\partial \bar{\mathbf{C}}} = \bar{\mathbf{C}}^e + \bar{\mathbf{C}}^v \quad (24)$$

where tensors  $\bar{\mathbf{C}}^e (= 4 \partial^2 \Psi / \partial \bar{\mathbf{C}} \partial \bar{\mathbf{C}})$  and  $\bar{\mathbf{C}}^v$  are hyperelastic and viscoelastic components of the viscoelastic tangent modulus, respectively.

By using  $\bar{\mathbf{S}}$  and  $\bar{\mathbf{C}}$ , the Cauchy stress tensor  $\boldsymbol{\sigma} (= \bar{\mathbf{J}}^{-1} \boldsymbol{\tau})$  and viscoelastic tangent modulus  $\mathbf{C}$  on the current configuration  $B_t$  are calculated by pushing  $\bar{\mathbf{S}}$  and  $\bar{\mathbf{C}}$  forward from  $\bar{B}_t$  to  $B_t$  respectively as follows

$$\boldsymbol{\sigma} = \bar{\mathbf{J}}^{-1} \mathbf{F}^{ve} \bar{\mathbf{S}} \mathbf{F}^{veT} \quad (25)$$

and

$$[\mathbf{c}]_{ijkl} = \bar{\mathbf{J}}^{-1} F_{il}^{ve} F_{jJ}^{ve} F_{kK}^{ve} F_{lL}^{ve} [\bar{\mathbf{C}}]_{IJKL}. \quad (26)$$

#### 4.1 Hyperelastic constitutive modelling

As a metric tensor,  $\bar{\mathbf{C}}$  is the fundamental strain tensor on  $\bar{B}_t$ . The function,  $\Psi$ , which takes into account the specified distribution of cellulose microfibrils, is expressed solely in terms of  $\bar{\mathbf{C}}$ . A multiplicative decomposition separates the deformation gradient  $\mathbf{F}^{ve}$  into volume-changing (dilational) and volume-preserving (distortional) parts. The strain measure of the dilational part is a Jacobian  $\bar{\mathbf{J}}$ . On the other hand, the strain measures of the distortional part are the modified viscoelastic right and left Cauchy-Green tensors,  $\hat{\mathbf{C}}$  and  $\hat{\mathbf{b}}$ , defined as

$$\hat{\mathbf{C}} = \bar{\mathbf{J}}^{-2/3} \bar{\mathbf{C}}, \quad \hat{\mathbf{b}} = \bar{\mathbf{J}}^{-2/3} \bar{\mathbf{b}} \quad (27)$$

which satisfy the conditions  $\det \hat{\mathbf{C}} = \det \hat{\mathbf{b}} = 1$ .

Based on experimental observations of biological tissues, a decoupled representation of the function,  $\Psi$ , which describes separately the volumetric and isochoric contributions, was suggested by Gasser *et al.* [56]. The general form of this decoupled representation of  $\Psi$  is presented as follows

$$\Psi(\bar{\mathbf{J}}, \hat{\mathbf{C}}, \bar{\mathbf{A}}) = \Psi_{vol}(\bar{\mathbf{J}}) + \Psi_{iso}(\hat{\mathbf{I}}_1, \hat{\mathbf{I}}_2, \hat{\mathbf{I}}_4, \hat{\mathbf{I}}_5) \quad (28)$$

where  $\bar{\mathbf{A}} = \bar{\mathbf{a}} \otimes \bar{\mathbf{a}}$  in which the vector  $\bar{\mathbf{a}}$  is defined by

$$\bar{\mathbf{a}} = \mathbf{F}^s \mathbf{a}_0, \quad (29)$$

Noting that  $\bar{\mathbf{a}}$  a unit vector in the present model since the growth law of  $\mathbf{F}^s$  (see flow rule (82)) ensures that microfibrils do not experience irreversible extension, i.e. growth in the fibre direction.

The four invariants  $\hat{I}_1, \hat{I}_2, \hat{I}_4, \hat{I}_5$  are defined as

$$\hat{I}_1(\hat{\mathbf{C}}) = \text{tr} \hat{\mathbf{C}}, \quad \hat{I}_2(\hat{\mathbf{C}}) = \frac{1}{2} \left[ (\text{tr} \hat{\mathbf{C}})^2 - \text{tr} \hat{\mathbf{C}}^2 \right], \quad \hat{I}_4(\hat{\mathbf{C}}, \bar{\mathbf{A}}) = \hat{\mathbf{C}} : \bar{\mathbf{A}} = \hat{\lambda}_a, \quad \hat{I}_5(\hat{\mathbf{C}}, \bar{\mathbf{A}}) = \hat{\mathbf{C}}^2 : \bar{\mathbf{A}}. \quad (30)$$

In the present modelling of cell wall, a particular free energy function [56] with a neo-Hookean isotropic part is used as follows

$$\begin{aligned} \Psi(\bar{J}, \hat{\mathbf{C}}, \bar{\mathbf{A}}) &= \Psi_{vol}(\bar{J}) + \Psi_{iso}(\hat{I}_1, \hat{I}_4) \\ &= \frac{1}{2} \kappa (\bar{J} - 1)^2 + \frac{1}{2} \mu (\hat{I}_1 - 3) + \frac{1}{2} \frac{\kappa_1}{\kappa_2} \left[ \exp\left(\kappa_2 (\hat{I}_4 - 1)^2\right) - 1 \right] \end{aligned} \quad (31)$$

where  $\kappa$  and  $\mu$  are interpreted as the bulk modulus and shear modulus of cell wall matrix, respectively, and  $\kappa_1$  and  $\kappa_2$  are parameters of the elastic response of cellulose microfibrils. The first and second terms on the right side of eqn. (31) define the isotropic hyperelastic response of cell wall matrix. The third term is obtained from a more general formulation suggested in Gasser *et al.* [56] by specifying the distribution of fibres.

It is noteworthy that, although the growth is a finite deformation (the wall enlarges by a factor from 10 to 100), the elastic strain is small (around 0.001) according to the experimental observation considered here [66]. If only the order of magnitude of the elastic strain is considered, a linear constitutive law for small strain elasticity is appropriate for representing the elastic response in cell wall. However, a constitutive model derived by combining small strain elasticity and finite strain growth leads to a hypoelasto-viscoplasticity model which is inferior to the hyperelasto-viscoplasticity model in dealing with the anisotropy and objectiveness [54]. Therefore the neo-Hookean free energy function (31) is adopted in the present study for obtaining a desirable frame-indifferent anisotropic model consistent with experimental observation.

The explicit expressions of  $\bar{\mathbf{S}}^e$ ,  $\bar{\mathbf{C}}^e$ ,  $\boldsymbol{\sigma}^e$  and  $\boldsymbol{\mathcal{C}}^e$  calculated from the specified function in eqn.(31) are shown in Table 1 in which  $\mathbf{I}$  and  $\mathbf{I}_{\bar{\mathbf{C}}^{-1}}$  are the fourth-order tensors with components  $(\mathbf{I})_{ijkl} = \frac{1}{2}(\delta_{ik}\delta_{jl} + \delta_{il}\delta_{jk})$  and  $(\mathbf{I}_{\bar{\mathbf{C}}^{-1}})_{ijkl} = (\bar{\mathbf{C}}_{ik}^{-1}\bar{\mathbf{C}}_{jl}^{-1} + \bar{\mathbf{C}}_{il}^{-1}\bar{\mathbf{C}}_{jk}^{-1})/2$ , respectively. The two coefficients  $\alpha_1$  and  $\alpha_2$  are defined as follows

$$\alpha_1 = (\hat{\lambda}_a - 1) \exp\left(\kappa_2 (\hat{\lambda}_a - 1)^2\right), \quad \alpha_2 = \left(1 + 2\kappa_2 (\hat{\lambda}_a - 1)^2\right) \exp\left(\kappa_2 (\hat{\lambda}_a - 1)^2\right). \quad (32)$$

**Table 1:** Stress tensor and elastic tangent modulus

Intermediate configuration description	Spatial description
Second Piola-Kirchhoff stress tensor	Cauchy stress tensor

$\bar{\mathbf{S}}^e = \kappa \bar{J} (\bar{J} - 1) \bar{\mathbf{C}}^{-1} + \mu \bar{J}^{-2/3} \text{DEV}[\mathbf{I}]$ $+ 2\kappa_1 \alpha_1 \bar{J}^{-2/3} \text{DEV}[\bar{\mathbf{A}}]$	$\boldsymbol{\sigma}^e = \kappa (\bar{J} - 1) \mathbf{I} + \mu \bar{J}^{-1} \text{dev} \left[ \hat{\mathbf{b}} \right]$ $+ 2\kappa_1 \alpha_1 \bar{J}^{-5/3} \text{dev}[\mathbf{A}]$
<p>Elastic tangent modulus.</p> $\bar{\mathbf{C}}^e = \kappa \bar{J} (2\bar{J} - 1) (\bar{\mathbf{C}}^{-1} \otimes \bar{\mathbf{C}}^{-1}) - 2\kappa \bar{J} (\bar{J} - 1) \mathbf{I}_{\bar{\mathbf{C}}^{-1}}$ $+ \frac{2}{3} \mu \bar{J}^{-2/3} \left\{ (\text{tr} \bar{\mathbf{C}}) \left[ \mathbf{I}_{\bar{\mathbf{C}}^{-1}} - \frac{1}{3} \bar{\mathbf{C}}^{-1} \otimes \bar{\mathbf{C}}^{-1} \right] \right.$ $\left. - \left[ \bar{\mathbf{C}}^{-1} \otimes \text{DEV}[\mathbf{I}] + \text{DEV}[\mathbf{I}] \otimes \bar{\mathbf{C}}^{-1} \right] \right\}$ $+ 2\kappa_1 \bar{J}^{-4/3} \left\{ \alpha_2 \text{DEV}[\bar{\mathbf{A}}] \otimes \text{DEV}[\bar{\mathbf{A}}] \right.$ $+ \frac{1}{3} \alpha_1 \hat{\lambda}_a \bar{J}^{4/3} \left[ \mathbf{I}_{\bar{\mathbf{C}}^{-1}} - \frac{1}{3} \bar{\mathbf{C}}^{-1} \otimes \bar{\mathbf{C}}^{-1} \right]$ $\left. - \frac{1}{3} \alpha_1 \bar{J}^{2/3} \left[ \bar{\mathbf{C}}^{-1} \otimes \text{DEV}[\bar{\mathbf{A}}] + \text{DEV}[\bar{\mathbf{A}}] \otimes \bar{\mathbf{C}}^{-1} \right] \right\}$	<p>Elastic tangent modulus</p> $\mathbf{c}^e = \kappa (2\bar{J} - 1) (\mathbf{I} \otimes \mathbf{I}) - 2\kappa (\bar{J} - 1) \mathbf{I}$ $+ \frac{2}{3} \mu \bar{J}^{-1} \left\{ \text{tr} \hat{\mathbf{b}} \left[ \mathbf{I} - \frac{1}{3} \mathbf{I} \otimes \mathbf{I} \right] \right.$ $\left. - \left[ \mathbf{I} \otimes \text{dev} \left[ \hat{\mathbf{b}} \right] + \text{dev} \left[ \hat{\mathbf{b}} \right] \otimes \mathbf{I} \right] \right\}$ $+ 2\kappa_1 \bar{J}^{-7/3} \left\{ \alpha_2 \text{dev}[\mathbf{A}] \otimes \text{dev}[\mathbf{A}] \right.$ $+ \frac{1}{3} \alpha_1 \hat{\lambda}_a \bar{J}^{4/3} \left[ \mathbf{I} - \frac{1}{3} \mathbf{I} \otimes \mathbf{I} \right]$ $\left. - \frac{1}{3} \alpha_1 \bar{J}^{2/3} \left[ \mathbf{I} \otimes \text{dev}[\mathbf{A}] + \text{dev}[\mathbf{A}] \otimes \mathbf{I} \right] \right\}$

#### 4.2 Evolution of viscoelastic internal variables

It is assumed that the internal variables  $\tilde{\mathbf{Q}}$  and  $\hat{\mathbf{Q}}$  evolve with the hyperelastic-stress-like driving forces,  $\tilde{\mathbf{S}}^\circ$  and  $\hat{\mathbf{S}}^\circ$ , in terms of the tensors

$$\hat{\mathbf{C}} = \tilde{J}^{-2/3} \tilde{\mathbf{C}} \quad \text{and} \quad \hat{\mathbf{C}} = \hat{J}^{-2/3} \hat{\mathbf{C}} \quad (33)$$

where the tensor  $\hat{\mathbf{C}}$  is defined as  $\hat{\mathbf{C}} = \hat{\mathbf{F}}^T \hat{\mathbf{F}}$ ,  $\tilde{J}$  and  $\hat{J}$  are the Jacobians defined as  $\tilde{J} = \det \tilde{\mathbf{F}}$  and  $\hat{J} = \det \hat{\mathbf{F}}$ , respectively. Thus  $\hat{\mathbf{C}}$  and  $\hat{\mathbf{C}}$  are the distortional parts of the tensors  $\tilde{\mathbf{C}}$  and  $\hat{\mathbf{C}}$ , respectively. However, as aforementioned in the kinematical model, the tensors  $\bar{\mathbf{C}}$  and  $\tilde{\mathbf{C}}$  are the metric tensors on the configurations  $\bar{B}_t$  and  $\tilde{B}_t$ , respectively (see Fig. 3). By contrast,  $\hat{\mathbf{C}}$  is not taken as a metric tensor. Therefore  $\hat{\mathbf{C}}$  is rewritten as

$$\hat{\mathbf{C}} = \bar{J}^{-2/3} \mathbf{F}^{veT} \hat{\mathbf{b}}^{-1} \mathbf{F}^{ve} \quad (34)$$

where  $\hat{\mathbf{b}}$  is defined as  $\hat{\mathbf{b}} = \tilde{J}^{-2/3} \tilde{\mathbf{b}}$  with  $\tilde{\mathbf{b}} = \tilde{\mathbf{F}} \tilde{\mathbf{F}}^T$ . By using eqn.(34) it can be proved that the invariants of tensor  $\hat{\mathbf{C}}$  can be expressed in terms of  $\hat{\mathbf{C}}$  and  $\hat{\mathbf{b}}$  as follows

$$\text{tr} \hat{\mathbf{C}} = \hat{\mathbf{C}} : \hat{\mathbf{b}}^{-1}, \quad \det \hat{\mathbf{C}} = \det \hat{\mathbf{C}} \det \hat{\mathbf{b}}^{-1}. \quad (35)$$

Based on the above discussion, the evolution equations of the two stress-like viscoelastic internal variables,  $\tilde{\mathbf{Q}}$  and  $\hat{\mathbf{Q}}$ , on  $\bar{B}_t$  are proposed in a form as

$$\dot{\tilde{\mathbf{Q}}} + \frac{1}{\tilde{\tau}} \tilde{\mathbf{Q}} = \frac{\tilde{\gamma}}{\tilde{\tau}} \tilde{\mathbf{S}}^\circ, \quad (36)$$

$$\dot{\hat{\mathbf{Q}}} + \frac{1}{\hat{\tau}} \hat{\mathbf{Q}} = \frac{\hat{\gamma}}{\hat{\tau}} \hat{\mathbf{S}}^\circ \quad (37)$$

where the hyperelastic-stress-like driving forces of the evolution,  $\tilde{\mathbf{S}}^\circ$  and  $\hat{\mathbf{S}}^\circ$ , are defined respectively as

$$\tilde{\mathbf{S}}^\circ = \hat{\mathbf{F}}^{-1} \tilde{\tilde{\mathbf{S}}}^\circ \hat{\mathbf{F}}^{-T} \quad \text{in which} \quad \tilde{\tilde{\mathbf{S}}}^\circ = 2 \frac{\partial W^\circ(\hat{\hat{\mathbf{C}}})}{\partial \hat{\hat{\mathbf{C}}}}, \quad (38)$$

$$\hat{\mathbf{S}}^\circ = 2 \frac{\partial W^\circ(\hat{\mathbf{C}})}{\partial \hat{\mathbf{C}}} = 2 \frac{\partial \tilde{W}^\circ(\hat{\mathbf{C}}, \hat{\mathbf{b}})}{\partial \hat{\mathbf{C}}}. \quad (39)$$

whereby the function  $W^\circ$  is the wall matrix's deviatoric contribution to the function  $\Psi$  (e.g.  $W^\circ(\square) = \frac{1}{2} \mu (\text{tr}(\square) - 3)$  given eqn.(31)),  $\tilde{\gamma}$  and  $\hat{\gamma}$  are two parameters defining the fractions of inelastic components in  $\mathbf{F}^{ve}$ , the temperature-dependent parameters,  $\tilde{\tau}$  and  $\hat{\tau}$ , are the characteristic times of viscoelasticity defined in the form of the Arrhenius equation

$$\tilde{\tau} = \tilde{\tau}_0 \exp(-Q_{ve}/R(T - T_{ve})), \quad \hat{\tau} = \hat{\tau}_0 \exp(-Q_{ve}/R(T - T_{ve})) \quad (40)$$

in which  $\tilde{\tau}_0$ ,  $\hat{\tau}_0$ ,  $T_{ve}$  and the viscoelastic activation energy  $Q_{ve}$  are the parameters obtained by fitting experimental data and  $R$  ( $= 8.314472 \text{ J/K mol}$ ) is the gas constant. It is noted that  $\tilde{\mathbf{S}}^\circ$  is defined by pulling back  $\tilde{\tilde{\mathbf{S}}}^\circ$  from  $\tilde{B}_t$  to  $\tilde{B}_t$  but  $\hat{\mathbf{S}}^\circ$  is defined directly on  $\hat{B}_t$ .

It is worth mentioning the limitation of equations (36) and (37). They are linear rate equations (linear viscoelasticity) and might not be appropriate to capture the response away from the thermodynamic equilibrium [67]. Numerical studies are needed to justify the model.

The convolution representations of the evolution eqns.(36) and (37) are expressed as

$$\tilde{\mathbf{Q}} = \frac{\tilde{\gamma}}{\tilde{\tau}} \int_{-\infty}^t \exp[-(t-s)/\tilde{\tau}] \tilde{\mathbf{S}}^\circ ds = \tilde{\gamma} [\tilde{\mathbf{S}}^\circ - \tilde{\mathbf{H}}] \quad (41)$$

$$\hat{\mathbf{Q}} = \frac{\hat{\gamma}}{\hat{\tau}} \int_{-\infty}^t \exp[-(t-s)/\hat{\tau}] \hat{\mathbf{S}}^\circ ds = \hat{\gamma} [\hat{\mathbf{S}}^\circ - \hat{\mathbf{H}}] \quad (42)$$

where the tensors  $\tilde{\mathbf{H}}$  and  $\hat{\mathbf{H}}$  are two algorithmic internal variables defined as [52]

$$\tilde{\mathbf{H}} = \int_{-\infty}^t \exp[-(t-s)/\tilde{\tau}] \frac{\partial \tilde{\mathbf{S}}^\circ}{\partial s} ds, \quad (43)$$

$$\hat{\mathbf{H}} = \int_{-\infty}^t \exp[-(t-s)/\hat{\tau}] \frac{\partial \hat{\mathbf{S}}^\circ}{\partial s} ds. \quad (44)$$

Substituting eqns.(43) and (44) into eqn.(22) yields the second Piola-Kirchhoff stress  $\bar{\mathbf{S}}$  as follows

$$\bar{\mathbf{S}} = \bar{\mathbf{S}}^e - \bar{J}^{-2/3} \left\{ \tilde{\gamma} \text{DEV}[\tilde{\mathbf{S}}^\circ - \tilde{\mathbf{H}}] + \hat{\gamma} \text{DEV}[\hat{\mathbf{S}}^\circ - \hat{\mathbf{H}}] \right\}. \quad (45)$$

Once evolution eqns. (36) and (37) are obtained, the two functions  $\tilde{\Phi}$  and  $\hat{\Phi}$  in eqn.(21) can be derived by using the method suggested by Simo and Hughes [52]. On the one hand, given the thermodynamic equilibrium of viscoelastic response, eqns.(36)-(39) lead to

$$\dot{\tilde{\mathbf{Q}}} = \mathbf{0} \rightarrow \tilde{\mathbf{Q}} = 2\tilde{\gamma} \frac{\partial W^\circ(\hat{\hat{\mathbf{C}}})}{\partial \hat{\hat{\mathbf{C}}}}, \quad (46)$$

$$\dot{\hat{\mathbf{Q}}} = \mathbf{0} \rightarrow \hat{\mathbf{Q}} = 2\bar{\gamma} \frac{\partial \tilde{W}^\circ(\hat{\mathbf{C}}, \hat{\mathbf{b}})}{\partial \hat{\mathbf{C}}}. \quad (47)$$

On the other hand, the driving conjugate thermodynamic forces of viscoelastic response are zero since no dissipation takes place at equilibrium. According to this postulation for thermodynamic equilibrium, eqn.(23) leads to the state equations

$$\bar{J}^{-2/3} \tilde{\mathbf{C}} = \frac{\partial \tilde{\Phi}}{\partial \tilde{\mathbf{Q}}}, \quad \hat{\mathbf{C}} = \frac{\partial \hat{\Phi}}{\partial \hat{\mathbf{Q}}} \quad (48)$$

Eqns.(23) and (48) precisely define the functions  $\tilde{\Phi}$  and  $\hat{\Phi}$  as the Legendre transformation of functions  $W^\circ$  and  $\tilde{W}^\circ$  respectively as

$$\tilde{\Phi}(\tilde{\mathbf{Q}}) = -\bar{\gamma} W^\circ(\hat{\mathbf{C}}) + \bar{J}^{-2/3} \tilde{\mathbf{C}} : \tilde{\mathbf{Q}}, \quad \hat{\Phi}(\hat{\mathbf{Q}}) = -\bar{\gamma} \tilde{W}^\circ(\hat{\mathbf{C}}, \hat{\mathbf{b}}) + \hat{\mathbf{C}} : \hat{\mathbf{Q}}. \quad (49)$$

Based on the viscoelastic evolution equations (41)-(45), the calculation and update algorithm of  $\bar{\mathbf{S}}$  and  $\bar{\mathbf{C}}^v$  is proposed in Appendix A. The evolution equations (36) and (37) are justified by modelling the different viscoelastic behaviours of cell wall in loading and unloading processes as shown in the case studies.

## 5 Growth law: A viscoplastic constitutive modelling

The cell wall growth is featured by the integration of the expansion driven by stress and volumetric growth by new material deposition. The strategy for obtaining an integrative growth model is outlined as follows. Firstly a decomposition of growth is used to characterise anisotropic kinematics of the growth and to identify the corresponding driving forces. Secondly, by using the decomposition of growth and taking into account the interplay between the decomposed components of growth, the yield function, flow rules, hardening law and evolution of cell wall thickness are modelled in a consistent framework of viscoplasticity. Thirdly, a numerical scheme is suggested to represent the integrative growth model in a discrete format.

### 5.1 The decomposition of growth and the driving forces of growth

To account for the growth anisotropy, it was proposed that cells have independent growth mechanisms in different principal directions [45]. Two hypotheses, namely turgor driven creep and new material deposition, are widely accepted to be the fundamental aspects of the anisotropic cell wall growth [9][45]. Based on these hypotheses, it is assumed that the growth of cell walls refers to two independent kinematics, the turgor-driven isochoric expansion and the plastic volumetric deformation. Thus a *decomposition of growth* is assumed here where the growth can be decomposed into two parts: (a) isochoric expansive growth without irreversible extension of the microfibrils (part I) and (b) volumetric growth without irreversible extension of the microfibrils (part II) (see Fig. 4). As the two parts of the growth are based on different mechanisms, the stress tensor is decomposed into the corresponding driving forces accordingly.

We start from the relatively simpler driving force of volumetric growth. To obtain the expression for the driving force of volumetric growth, a spatial stress tensor,  $\boldsymbol{\tau}^A$ , is introduced as

$$\boldsymbol{\tau}^A = \boldsymbol{\tau} - \left\{ \boldsymbol{\tau} : \tilde{\mathbf{A}} \right\} \tilde{\mathbf{A}} \quad (50)$$

where  $\tilde{\mathbf{A}} = \tilde{\mathbf{a}} \otimes \tilde{\mathbf{a}}$ . The *effective* driving force is defined as

$$\boldsymbol{\tau}_{vol}(\boldsymbol{\tau}) = \text{tr}\boldsymbol{\tau}^A \quad (51)$$

for volumetric growth. Then the corresponding tensor of driving force is defined on  $B_t$  as

$$\boldsymbol{\tau}_{vol} = \frac{1}{3}\boldsymbol{\tau}_{vol}\mathbf{I}. \quad (52)$$

It can be proved that  $\boldsymbol{\tau}^A$  satisfies the condition of no growth in the direction of the microfibrils direction, i.e.  $\boldsymbol{\tau}^A : \mathbf{A} = 0$ .

On the other hand, the driving force of expansive growth is defined on  $B_t$  as

$$\boldsymbol{\tau}^{dev} = \boldsymbol{\tau} - \frac{3}{2}\left[\boldsymbol{\tau}_{vol} + \boldsymbol{\tau}_{\lambda_a}\right] = \boldsymbol{\tau} - \frac{1}{2}\left[\left\{\text{tr}\boldsymbol{\tau}^A\right\}\mathbf{I} + 3\left\{\boldsymbol{\tau} : \mathbf{R}_{\lambda_a}\right\}\tilde{\mathbf{A}}\right] \quad (53)$$

where  $\boldsymbol{\tau}_{\lambda_a}$  is

$$\boldsymbol{\tau}_{\lambda_a} = \tau_{\lambda_a}\tilde{\mathbf{A}} \quad \text{with } \tau_{\lambda_a}(\boldsymbol{\tau}) = \boldsymbol{\tau} : \mathbf{R}_{\lambda_a} \quad (54)$$

in which the tensor  $\mathbf{R}_{\lambda_a}$  is defined as  $\mathbf{R}_{\lambda_a} = \text{dev}\left[\tilde{\mathbf{A}}\right]$ . It can be proved that the spatial stress tensor  $\boldsymbol{\tau}^{dev}$  satisfies the conditions

$$\boldsymbol{\tau}^{dev} : \mathbf{A} = 0, \quad \text{tr}\boldsymbol{\tau}^{dev} = 0. \quad (55)$$

Eqn.(55) indicates that stress tensor  $\boldsymbol{\tau}^{dev}$  is the driving force of expansive growth because neither plastic volumetric deformation nor irreversible microfibrils extension takes place under this driving force.

With eqns.(52) and (53) obtained, a set of stress tensors,  $\boldsymbol{\tau}^{dev}$  and  $\boldsymbol{\tau}_{vol}$ , which correspond to the turgor-driven expansion and volumetric growth respectively, is taken as the set of driving forces of cell wall growth. These stress tensors play a similar role as the standard deviatoric stress tensor,  $\text{dev}[\boldsymbol{\sigma}]$ , in the  $J_2$ -viscoplasticity theory and are the fundamental tensors for establishing the yield criterion and plastic flow rule. By mapping back from  $B_t$  onto  $\bar{B}_t$ , tensors  $\bar{\mathbf{S}}^{DEV}$  and  $\bar{\mathbf{S}}_{vol}$ , which are the counterparts of  $\boldsymbol{\tau}^{dev}$  and  $\boldsymbol{\tau}_{vol}$  on  $\bar{B}_t$ , are defined respectively as

$$\bar{\mathbf{S}}^{DEV} = \bar{\mathbf{S}} - \frac{1}{2}\left[\left\{\text{Tr}\bar{\mathbf{S}}^A\right\}\bar{\mathbf{C}}^{-1} + \frac{3}{\lambda_a}\left\{\bar{\mathbf{S}} : \bar{\mathbf{R}}_{\lambda_a}\right\}\bar{\mathbf{A}}\right], \quad (56)$$

$$\bar{\mathbf{S}}_{vol} = \frac{1}{3}\left\{\text{Tr}\bar{\mathbf{S}}^A\right\}\bar{\mathbf{C}}^{-1} \quad (57)$$

where  $\bar{\mathbf{S}}^A$  is defined by pulling  $\boldsymbol{\tau}^A$  back onto  $\bar{B}_t$  as

$$\bar{\mathbf{S}}^A = \bar{\mathbf{S}} - \frac{1}{\lambda_a^2}\left\|\bar{\mathbf{S}}\right\|_{\bar{\mathbf{a}}}\bar{\mathbf{A}} \quad (58)$$

in which the function  $\left\|\left(\square\right)\right\|_{\bar{\mathbf{a}}}$  is defined on  $\bar{B}_t$  as

$$\left\|\left(\square\right)\right\|_{\bar{\mathbf{a}}} = \left[\bar{\mathbf{C}}\left(\square\right)\bar{\mathbf{C}}\right] : \bar{\mathbf{A}}, \quad (59)$$

and tensor  $\bar{\mathbf{R}}_{\lambda_a} = \hat{\mathbf{A}} - \frac{1}{3}\bar{\mathbf{C}}$  is the counterpart of  $\mathbf{R}_{\lambda_a}$  on  $\bar{B}_t$  in which  $\hat{\mathbf{A}} = \mathbf{F}^{eT}\tilde{\mathbf{A}}\mathbf{F}^e$ .

Similar to its counterpart  $\boldsymbol{\tau}^{dev}$ , the stress tensor  $\bar{\mathbf{S}}^{DEV}$  satisfies the conditions equivalent to eqn.(55) as follows

$$\|\bar{\mathbf{S}}^{DEV}\|_{\bar{\mathbf{a}}} = 0, \quad \text{Tr}\bar{\mathbf{S}}^{DEV} = 0. \quad (60)$$

It is noted that the tensor  $\boldsymbol{\tau}^{dev}$  is exactly the same as the deviatoric stress tensor suggested by Spencer [68] in infinitesimal strain format restricted to a composite containing a single family of microfibrils. Here Spencer's formulation is extended into a finite strain model. For convenience,  $\boldsymbol{\tau}^{dev}$  and  $\bar{\mathbf{S}}^{DEV}$  are referred to as Spencer's deviatoric stress tensors on  $B_t$  and  $\bar{B}_t$ , respectively.

## 5.2 Yield criterion

Due to their independent growth mechanisms, the two parts of the growth, i.e. isochoric expansive growth and volumetric growth, can have their own yield functions. However, restricting attention to the hypothesis that volumetric growth passively follows expansive growth to maintain the strength of the cell wall, we assume that isochoric expansion is solely responsible for the plastic yielding. Therefore the yielding criterion of the integrative model only depends on Spencer's deviatoric stress  $\bar{\mathbf{S}}^{DEV}$  (or  $\boldsymbol{\tau}^{dev}$ ).

Following Spencer's invariant theory [68], two invariants of Spencer's deviatoric stress tensor can be defined as

$$\bar{J}_1(\bar{\mathbf{S}}^{DEV}, \bar{\mathbf{a}}/\sqrt{\lambda_a}) = \frac{1}{\lambda_a} \|\bar{\mathbf{S}}^{DEV} \bar{\mathbf{C}}\bar{\mathbf{S}}^{DEV}\|_{\bar{\mathbf{a}}} \equiv (\boldsymbol{\tau}^{dev} \tilde{\mathbf{a}}) \cdot (\boldsymbol{\tau}^{dev} \tilde{\mathbf{a}}) = \tilde{J}_1(\boldsymbol{\tau}^{dev}, \tilde{\mathbf{a}}) \quad (61)$$

and

$$\bar{J}_2(\bar{\mathbf{S}}^{DEV}) = \text{Tr}(\bar{\mathbf{S}}^{DEV} \bar{\mathbf{C}}\bar{\mathbf{S}}^{DEV}) \equiv \boldsymbol{\tau}^{dev} : \boldsymbol{\tau}^{dev} = \tilde{J}_2(\boldsymbol{\tau}^{dev}). \quad (62)$$

The invariant  $\bar{J}_1$  (or  $\tilde{J}_1$ ) is a fibre-dependent invariant. On the other hand,  $\bar{J}_2$  (or  $\tilde{J}_2$ ) is the natural counterpart of  $J_2 (= \frac{1}{2} \text{dev}[\boldsymbol{\tau}] : \text{dev}[\boldsymbol{\tau}])$  in the classical  $J_2$ -viscoplasticity theory. Based on this observation, a natural generalization of the yield function for isochoric expansive growth which is consistent with the classical von Mises yield condition is written as

$$f_{dev}(\bar{\mathbf{S}}^{DEV}, \bar{\mathbf{a}}/\sqrt{\lambda_a}, \alpha) = \frac{\bar{J}_1}{Y_1^2} + \frac{\bar{J}_2}{Y_2^2} - (1 + h(\alpha)) \equiv \frac{\tilde{J}_1}{Y_1^2} + \frac{\tilde{J}_2}{Y_2^2} - (1 + h(\alpha)) = \tilde{f}_{dev}(\boldsymbol{\tau}^{dev}, \tilde{\mathbf{a}}, \alpha) \quad (63)$$

where  $Y_1$  and  $Y_2$  are two yield parameters with dimensions of stress, and  $h$  is a scalar hardening function in terms of the hardening parameter  $\alpha$ . It is noted that the only remaining invariant of  $\boldsymbol{\tau}^{dev}$ , i.e.  $\text{tr}((\boldsymbol{\tau}^{dev})^3)$ , is not considered here according to plasticity theory. Therefore, eqn.(63) already contains all of the admissible invariants of Spencer's deviatoric stress  $\bar{\mathbf{S}}^{DEV}$  (or  $\boldsymbol{\tau}^{dev}$ ).

Here the yield function is proposed based on the general methodology in plasticity to generalise the uniaxial 1D model into a 3D model. On the one hand, the Lockhart equation is taken as the 1D model summarising the experimental observations. On the other hand, the local 3D driving force  $\bar{\mathbf{S}}^{DEV}$  (or  $\boldsymbol{\tau}^{dev}$ ) is established based on the mechanisms of the anisotropic growth. Then yield function (63) is presented in terms of the invariants of  $\bar{\mathbf{S}}^{DEV}$  (or  $\boldsymbol{\tau}^{dev}$ ) and is consistent with Lockhart equation.

The justification of eqn.(63) is two-folds. Firstly, stress  $\bar{\mathbf{S}}^{DEV}$  (or  $\boldsymbol{\tau}^{dev}$ ) as a driving force of expansive growth is consistent with the existing hypotheses for the growth [8][11][12]. A linear combination of their invariants in eqn.(63) already covers all the admissible linear formulations of the yield function. Therefore eqn.(63) is expected to be able to represent the general yielding behaviours of the cell wall. Secondly, eqn.(63) is consistent with Lockhart equation (1) to predict the yield condition of the elongation of the cell wall in experimental observations, i.e. the threshold of turgor pressure for growth, as shown in the case studies of the present work.

### 5.3 Overstress functions

In the present study, a flow rule using the Perzyna model [52] is suggested which involves the overstress function defined in the space of invariants of stress. Corresponding to the set of driving forces  $\boldsymbol{\tau}^{dev}$  and  $\boldsymbol{\tau}_{vol}$  (or  $\bar{\mathbf{S}}^{DEV}$  and  $\bar{\mathbf{S}}_{vol}$ ) proposed in the preceding discussion, there are two separate overstress functions.

First, the overstress function for isochoric expansive growth should be defined in terms of Spencer's deviatoric stress tensor  $\bar{\mathbf{S}}^{DEV}$ . A naturally generalised overstress function is defined in terms of the minimum distance between the current stress point, which is outside the yield surface, and the yield surface in the space of invariants,  $S_{\bar{\mathbf{J}}} = \left\{ \sqrt{\bar{J}_1}, \sqrt{\bar{J}_2} \right\} \subseteq R^+ \times R^+$ , in which  $R^+$  denotes the set of non-negative real numbers.

As shown in Fig. 5, given a point  $\bar{\mathbf{J}} = \left( \sqrt{\bar{J}_1}, \sqrt{\bar{J}_2} \right) \in S_{\bar{\mathbf{J}}}$ , a measure function between this point and any other point  $\tilde{\boldsymbol{\theta}} = \left( \tilde{\theta}_1, \tilde{\theta}_2 \right) \in S_{\bar{\mathbf{J}}}$  is defined as

$$\tilde{\phi}(\tilde{\boldsymbol{\theta}}, \bar{\mathbf{J}}) = \sqrt{(\bar{\mathbf{J}} - \tilde{\boldsymbol{\theta}}) \cdot (\bar{\mathbf{J}} - \tilde{\boldsymbol{\theta}})} \quad \forall \tilde{\boldsymbol{\theta}} \in S_{\bar{\mathbf{J}}}. \quad (64)$$

Then a distance function,  $\phi(\bar{\boldsymbol{\theta}}, \bar{\mathbf{J}})$ , representing the minimum distance between the given point  $\bar{\mathbf{J}}$  and the yield surface  $f_{dev} = 0$  can be defined as

$$\left. \begin{aligned} \phi(\bar{\boldsymbol{\theta}}, \bar{\mathbf{J}}) &= \min_{\tilde{\boldsymbol{\theta}} \in S_{\bar{\mathbf{J}}}} \tilde{\phi}(\tilde{\boldsymbol{\theta}}, \bar{\mathbf{J}}) \\ s.t. \quad f_{dev}(\tilde{\boldsymbol{\theta}}, \alpha) &= \frac{\tilde{\theta}_1^2}{Y_1^2} + \frac{\tilde{\theta}_2^2}{Y_2^2} - (1 + h(\alpha)) = 0 \end{aligned} \right\} \quad (65)$$

where *s.t.* denotes 'subject to (the constraint)'. The point  $\bar{\boldsymbol{\theta}}$  is the closest point projection of  $\bar{\mathbf{J}}$  onto the yield surface.

Solving the constrained minimum problem (65) yields the distance function as

$$\phi(\bar{\boldsymbol{\theta}}, \bar{\mathbf{J}}) = -\theta \sqrt{\frac{\bar{J}_1}{(Y_1^2 - \theta)^2} + \frac{\bar{J}_2}{(Y_2^2 - \theta)^2}} \quad (66)$$

where the Lagrange multiplier  $\theta$  is one of the real roots of a quartic equation

$$(1+h)(\theta - Y_1^2)^2 (\theta - Y_2^2)^2 - \bar{J}_2 Y_2^2 (\theta - Y_1^2)^2 - \bar{J}_1 Y_1^2 (\theta - Y_2^2)^2 = 0 \quad (67)$$

which, by comparison with other real roots, gives the smallest non-negative  $\phi$ . Thus the overstress function for isochoric expansive growth can be defined as

$$\bar{\phi}_{dev} = \begin{cases} 0 & \text{if } f_{dev}(\bar{\mathbf{S}}^{DEV}, \bar{\mathbf{a}}/\sqrt{\lambda_a}, \alpha) \leq 0 \\ \phi^m & \text{if } f_{dev}(\bar{\mathbf{S}}^{DEV}, \bar{\mathbf{a}}/\sqrt{\lambda_a}, \alpha) > 0 \end{cases} \quad (68)$$

where  $m$  is a rate-sensitivity exponent. The overstress function  $\bar{\phi}_{dev}$  is *implicitly* defined as a function of yield function  $f_{dev}$ .

Second, the overstress functions for volumetric growth are defined explicitly, following the classical  $J_2$ -viscoplasticity theory, as the functions of the corresponding yield-surface-like function  $f_{vol}$  as

$$\bar{\phi}_{vol} = \langle f_{vol} \rangle / 2 \quad (69)$$

where the yield-surface-like function of volumetric growth,  $f_{vol}$ , is suggested as

$$f_{vol}(\bar{\mathbf{S}}^A) = \bar{I}_2(\bar{\mathbf{S}}^A) - Y_3 \equiv I_2(\boldsymbol{\tau}^A) - Y_3 = \tilde{f}_{vol}(\boldsymbol{\tau}^A) \quad (70)$$

in which  $Y_3$  is the ‘yield threshold’ and the second invariant  $\bar{I}_2$  (or  $I_2$ ) is defined as

$$\bar{I}_2(\bar{\mathbf{S}}^A) = \frac{1}{2} \left( (\text{Tr} \bar{\mathbf{S}}^A)^2 - \text{Tr}(\bar{\mathbf{S}}^A \bar{\mathbf{C}} \bar{\mathbf{S}}^A) \right) \equiv \frac{1}{2} \left( (\text{tr} \boldsymbol{\tau}^A)^2 - \boldsymbol{\tau}^A : \boldsymbol{\tau}^A \right) = I_2(\boldsymbol{\tau}^A). \quad (71)$$

Therefore, functions  $\bar{\phi}_{dev}$  and  $\bar{\phi}_{vol} = \langle f_{vol} \rangle / 2$  are the overstress functions for the expansive and volumetric growths, respectively.

#### 5.4 Flow rule

The expansive growth of cell wall is generally dominated by the elongation in a particular direction. Based on this fact, by adopting the assumption that the plastic spin,  $\text{skw} \bar{\mathbf{L}}^g$ , vanishes, it is sufficient to specify the flow rule as the evolution of  $\bar{\mathbf{D}}^g$ .

Following the penalty formulation proposed by Simo and Hughes [52], the principle of maximum dissipation corresponding to inequality (20)<sub>1</sub> is represented as an unconstrained minimization problem as follows

$$\begin{aligned} & \min_{(\bar{\mathbf{S}}, q) \in \mathcal{S} \times \mathcal{R}^1} \left\{ -\mathbf{D}_g^*(\bar{\mathbf{S}}, q, \bar{\mathbf{D}}^g, \dot{\boldsymbol{\alpha}}) \right\} \\ & \mathbf{D}_g^*(\bar{\mathbf{S}}, q, \bar{\mathbf{D}}^g, \dot{\boldsymbol{\alpha}}) = \mathbf{D}_g(\bar{\mathbf{S}}, q, \bar{\mathbf{D}}^g, \dot{\boldsymbol{\alpha}}) - \frac{1}{\eta} \mathbf{F}_g(\bar{\mathbf{S}}, q) \end{aligned} \quad (72)$$

where  $\mathcal{S}$  denotes the vector space of symmetric second order tensors,  $\eta$  is so-called penalty function, and the dissipation potential  $\mathbf{F}_g$  is suggested as

$$\mathbf{F}_g(\bar{\mathbf{S}}, q) = \gamma^+(\bar{\phi}_{dev}) + \beta_1 \gamma^+(\bar{\phi}_{vol}) \quad (73)$$

in which  $\beta_1$  is a weighted parameter and the function  $\gamma^+(\square)$  is defined as [52]

$$\gamma^+(x) = \begin{cases} \frac{1}{2}x^2 & \text{if } x \geq 0 \\ 0 & \text{if } x < 0 \end{cases}. \quad (74)$$

Solving the minimization problem (72) yields two optimality conditions

$$-\frac{\partial \mathbf{D}_g^*}{\partial \bar{\mathbf{S}}} = 0, \quad -\frac{\partial \mathbf{D}_g^*}{\partial q} = 0. \quad (75)$$

The first optimality condition  $-\partial \mathbf{D}_g^* / \partial \bar{\mathbf{S}} = 0$  yields a general format of growth flow rule on  $\bar{B}_t$  in the following form

$$\bar{\mathbf{D}}^g = \dot{\lambda} \frac{\partial \bar{\phi}_{dev}}{\partial \bar{\mathbf{S}}} + \dot{\lambda}_{vol} \frac{\partial \bar{\phi}_{vol}}{\partial \bar{\mathbf{S}}} \quad (76)$$

where the rates of effective viscoplastic strains,  $\dot{\lambda}$  and  $\dot{\lambda}_{vol}$ , are formulated as

$$\dot{\lambda} = \frac{\bar{\phi}_{dev}}{\eta}, \quad \dot{\lambda}_{vol} = \frac{\bar{\phi}_{vol}}{\eta/\beta_1}. \quad (77)$$

The penalty function  $\eta$  is recognised as a temperature-dependent viscosity which is defined in the form of the Arrhenius equation

$$\eta = \eta_0 \exp(-Q/R(T - T_0)) \quad (78)$$

in which  $\eta_0$ ,  $T_0$  and growth activation energy  $Q$  are three parameters obtained by fitting experimental data. Function  $\eta/\beta_1$  is the matrix bulk viscosity. Eqn.(78) is supported by the experimental finding reported by Proseus *et al.* [69]. Moreover, eqn.(78) is also consistent with the conclusion proposed by Thomas *et al.* [70] that the growth reduction at low temperature exhibited by leaves of *Lolium temulentum* by low temperature is due to changes in cell wall rheology.

By taking the derivative of  $\bar{\phi}_{dev}$  and  $\bar{\phi}_{vol}$  with respect to the Kirchhoff stress  $\boldsymbol{\tau}$  and then mapping back from  $B_t$  onto  $\bar{B}_t$ , two derivatives,  $\partial \bar{\phi}_{dev} / \partial \bar{\mathbf{S}}$  and  $\partial \bar{\phi}_{vol} / \partial \bar{\mathbf{S}}$ , are obtained as [51]

$$\text{sym} \bar{\mathbf{R}}^* = \frac{\partial \bar{\phi}_{dev}}{\partial \bar{\mathbf{S}}} = \beta_3 \left[ \hat{\mathbf{A}} \bar{\boldsymbol{\Sigma}}^{DEV} + \left( \hat{\mathbf{A}} \bar{\boldsymbol{\Sigma}}^{DEV} \right)^T \right] + 4\beta_4 \text{sym} \bar{\boldsymbol{\Sigma}}^{DEV}, \quad (79)$$

$$\bar{\mathbf{R}}_{vol}^* = \frac{\partial \bar{\phi}_{vol}}{\partial \bar{\mathbf{S}}} = \{ \text{Tr} \bar{\mathbf{S}}^A \} \bar{\mathbf{R}}_{vol} - \bar{\mathbf{C}} \bar{\mathbf{S}}^A \bar{\mathbf{C}} \quad (80)$$

where  $\bar{\boldsymbol{\Sigma}}^{DEV} = \bar{\mathbf{S}}^{DEV} \bar{\mathbf{C}}$  is a form of the Mandel stress [71][72], tensor  $\bar{\mathbf{R}}_{vol}$  is defined as  $\bar{\mathbf{R}}_{vol} = \bar{\mathbf{C}} - \hat{\mathbf{A}}$ , and the two functions,  $\beta_3$  and  $\beta_4$ , are defined as

$$\beta_3 = m\phi^{m-1} \left( \frac{\partial \phi}{\partial \bar{J}_1} + \mathcal{G}_1 \frac{\partial \phi}{\partial \theta} \right), \quad \beta_4 = m\phi^{m-1} \left( \frac{\partial \phi}{\partial \bar{J}_2} + \mathcal{G}_2 \frac{\partial \phi}{\partial \theta} \right) \quad (81)$$

in which  $\mathcal{G}_1$  and  $\mathcal{G}_2$  are defined in (B2). The calculation of eqn.(79) refers to the derivative of function  $\phi$  which is discussed in Appendix B.

The flow rule in eqns. (79) and (80) indicates a consistency between the present model and the growth theory based on Eshelby (energy-momentum) tensor and its degenerate form, i.e. Mandel stress [73].

On the one hand, Mandel stress  $\bar{\Sigma}^{DEV}$  is the driving force for the isochoric expansion. On the other hand, the flow direction of volumetric growth,  $\bar{\mathbf{R}}_{vol}^*$ , is consistent with the first order volumetric growth model suggested by Epstein and Maugin [46][74] in which transpland (growth) tensor of volumetric growth is a function in terms of the static Eshelby stress tensor,  $\{\Psi\}\bar{\mathbf{C}} - \bar{\mathbf{C}}\bar{\mathbf{S}}\bar{\mathbf{C}}$ .

Substituting eqns. (79) and (80) into the right side of eqn. (76), we obtain a flow rule of cell wall growth as

$$\bar{\mathbf{D}}^g = \dot{\lambda}_{sym}\bar{\mathbf{R}}^* + \dot{\lambda}_{vol}\bar{\mathbf{R}}_{vol}^*. \quad (82)$$

From the point of view of biology, it is worth mentioning that the local plastic flow,  $\bar{\mathbf{D}}^g$ , plays the role of regulating the global growth of cell wall in a particular direction. Plant cells rarely enlarge isotropically; instead, they grow preferentially in a single direction [5]. Therefore, being consistent with the biological mechanisms and taking advantage of the multiplicative decomposition (6), the plastic flow rule defined by eqn. (82) is used to achieve the anisotropic growth in the present model. The anisotropic growth observed in experiments, i.e. elongation in the longitudinal direction, stability of wall thickness in the radial direction, and ignorable growth in the circumferential direction, can be modelled by the flow rule (82) as shown in the case studies in this paper, which justify the flow rule. Furthermore, since it only depends on the local stress and fibre direction, the flow rule (82) can be applied to cells with different shapes.

### 5.5 Interplay between isochoric expansion and volumetric growth

Hitherto, the only interplay between the expansive and volumetric growths taken into account is the assumption that the yield surface of the integrative system is dominated by expansive growth. In order to obtain an integrative growth model, more interplays between the parts I and II of the growth are discussed at both molecular level and macroscopic level, which lead to the hardening law and the control equation of wall thickness.

#### 5.5.1 Hardening law

The second optimality condition,  $-\partial\mathbf{D}_g^*/\partial q = 0$ , in eqn. (75) together with eqn. (77) and the chain rule yield the following hardening law

$$\dot{\alpha} = \frac{1}{K} \frac{\partial\bar{\phi}_{dev}}{\partial\alpha} \dot{\lambda} \quad (83)$$

where the function  $\partial\bar{\phi}_{dev}/\partial\alpha$  ( $\bar{\phi}_{dev} \neq 0$ ) is calculated by using eqns. (53) and (B4) as

$$\frac{\partial\bar{\phi}_{dev}}{\partial\alpha} = m\bar{\phi}^{m-1}\mathcal{G}_h \frac{\partial\bar{\phi}}{\partial\theta} \frac{\partial h}{\partial\alpha} \quad (84)$$

in which  $\mathcal{G}_h$  is defined in eqn.(B2) in Appendix B.

The evolution of the hardening parameters in eqn.(83) depends on the specified hardening function  $h(\alpha)$ . However, instead of constructing this function, a direct mechanism-based method was suggested to obtain the evolution equation of  $\alpha$  in our previous publication [51]. Being consistent with the mechanism proposed by Proseus and Boyer [75], we suggested that the hardening parameter  $\alpha$  is taken as the *number fraction* of the load-bearing cross-links in a representative element on  $\bar{\mathbf{B}}_t$ , which is defined as the ratio of the number of the plastic load-bearing cross-links to the total number

of the cross-links associated with growth. The mechanism-based method leads to a phenomenological hardening law as follows

$$\dot{\alpha} = (h_1 + h_2\alpha)\dot{\lambda} \quad (85)$$

where  $h_1$  represents the effect of strain hardening due to the increase in the number fraction of the load-bearing cross-links when the cell wall is loaded, and  $h_2$  represents the effect of re-stiffening due to the capacity of plant to add new structural components and to repair many forms of mechanical damage [76]. The corresponding mechanism-based analysis indicates that  $h_1$  is always positive and  $h_2$  is negative for living cells but vanishes for isolated walls. Moreover, parameter  $h_1$  of the isolated wall is larger than that of the corresponding living cell.

The specific interplay between parts I and II of growth at the molecular scale on which the hardening law (85) is based can be explained briefly as follows. The evolution equation (85) derived from the assumption that the irreversible change of the number of load-bearing cross-links is taken as the sole mechanism of hardening in the present model. For the isolated wall there is no other mechanism to counter the hardening mechanism, so that expansive growth decelerates and then stops inevitably ( $h_2 = 0$ ). By contrast, new material deposition, which is usually considered as a process maintaining the strength of the wall, also plays the role of countering the hardening to create a growth-sustaining activity at molecular scale in the living cell ( $h_2 < 0$ ) [75].

With eqn.(85), the function  $h(\alpha)$  in the yield function in eqn.(63) is suggested to be  $h = \alpha$  which is simple enough for verifying the suggested evolution equation of  $\alpha$ .

### 5.5.2 Evolution of the wall thickness

In contrast to the dramatic change of the area of wall surface during growth, wall thickness is relatively stable. Experimental observation has indicated that the wall may become thinner or thicker perhaps by as much as two-fold [14][15]. This observation leads to the wall thickness hypotheses as the geometric constraints to represent the interaction between the expansion and the new material deposition in which the rate of effective strain  $\dot{\lambda}_{vol}$  is directly governed by  $\dot{\lambda}$ .

Instead of the hypothesis of constant wall thickness used by some other researchers [7][36], a relaxed assumption that the cell wall can dynamically stabilise its thickness was proposed by the present authors [51] for modelling some experimental observations reported by Taiz [14], Kutschera [15], and Proseus *et al.* [66]. The assumption yields the evolution equation

$$\left. \frac{\partial \dot{\lambda}_{vol}}{\partial t} \right|_{X \text{ fixed}} = - \frac{\dot{\lambda}_{vol} - \zeta \dot{\lambda}}{t_c} \quad (86)$$

where  $t_c$  is a characteristic time indicating the response time of  $\dot{\lambda}_{vol}$  to the change of  $\dot{\lambda}$ ,  $\zeta = -(\bar{\mathbf{n}} \cdot \text{sym} \bar{\mathbf{R}}^* \cdot \bar{\mathbf{n}}) / (\bar{\mathbf{n}} \cdot \bar{\mathbf{R}}_{vol}^* \cdot \bar{\mathbf{n}})$  in which  $\bar{\mathbf{n}} = \mathbf{F}^{e-1} \mathbf{n}$  and vector  $\mathbf{n}$  is the principal direction associated the minimum principal stress which roughly aligns with the unit normal vector perpendicular to the current cell wall surface. In the equilibrium state, i.e.  $\partial \dot{\lambda}_{vol} / \partial t \big|_{X \text{ fixed}} = 0$ , eqn.(86) reduces to the assumption of constant wall thickness, i.e.  $\mathbf{n} \cdot \mathbf{D}^g \cdot \mathbf{n} = 0$ .

With the initial condition of  $\dot{\lambda}_{vol}|_{t=0} = 0$ , the approximate solution of eqn. (86) at  $t = t_{n+1} = t_n + \Delta t$  by using the Eulerian forward differential formulation is

$$\dot{\lambda}_{vol}(t_{n+1})|_{X \text{ fixed}} = \tilde{\zeta}_n \dot{\lambda}|_{t=t_{n+1}}, \quad \tilde{\zeta}_n = \left( \frac{\dot{\lambda}_{vol}}{\dot{\lambda}} - \zeta \right) \Big|_{t=t_n} e^{-\Delta t/t_c} + \zeta|_{t=t_n}. \quad (87)$$

Eqn. (87) represents the interaction between the isochoric expansion and volumetric growth at macroscopic scale for the living cells. For completeness,  $\tilde{\zeta}_n$  is set to be zero for the isolated walls. It is noted that eqn.(87) is applied only to plant cells during their growth phase.

## 5.6 Numerical scheme

Hitherto, an integrative model of *in vivo* cell wall growth is presented with its structure summarised as follows. By assuming that the plastic extension of microfibrils is negligible, the integrative model is sufficiently defined by the yield function (63) of the isochoric expansion, the flow rule (82) of the isochoric expansion and volumetric growth, the hardening law (85), and the control equation of wall thickness (87). The numerical schemes in classical viscoplasticity can be implemented directly in this integrative model to obtain a growth model in a discretised format.

### 5.6.1 Stress update algorithm

Due to the fact that the growth direction usually does not undergo sharp changes, the semi-implicit stress update algorithm on  $\bar{B}_t$  suggested by Moran *et al.* [53] is adopted in the present numerical implementation. The algorithm, which is a specific return-mapping algorithm, involves two stages; the elastic predictor (trial solution) obtained by freezing the plastic flow, followed by the plastic corrector driven by exactly satisfying eqn. (77) while the total strain and the plastic flow direction are fixed. The algorithm for the present fibre-reinforced model is summarized as follows:

- (i) Geometric update from a given incremental displacement  $\mathbf{u}$

$$\varphi_{n+1} = \varphi_n + \mathbf{u} \quad (88)$$

$$\mathbf{F}_{n+1} = \partial \varphi_{n+1} / \partial \mathbf{X} \quad (89)$$

- (ii) Given  $\mathbf{F}_{n+1}$ ,  $\mathbf{F}_n$ ,  $\mathbf{F}_n^g$ ,  $\tilde{\mathbf{F}}_n$ ,  $\hat{\mathbf{F}}_n$ ,  $\bar{\mathbf{S}}_n$ ,  $\alpha_n$  and  $\Delta t$ , update  $\mathbf{F}_{n+1}^g$ ,  $\bar{\mathbf{a}}_{n+1}$ ,  $\bar{\mathbf{n}}_{n+1}$ ,  $\tilde{\mathbf{F}}_{n+1}$ ,  $\hat{\mathbf{F}}_{n+1}$ ,  $\bar{\mathbf{S}}_{n+1}$  and  $\alpha_{n+1}$  by setting

$$\bar{\mathbf{R}}_n = \bar{\mathbf{R}}_n^* + \tilde{\zeta}_n \bar{\mathbf{R}}_{vol}^*(t_n) \quad (90)$$

$$\mathbf{F}_{n+1}^g = (\mathbf{I} + \Delta \lambda_n \bar{\mathbf{R}}_n) \mathbf{F}_n^g \quad (91)$$

$$\mathbf{F}_{n+1}^{ve} = \mathbf{F}_{n+1} \mathbf{F}_{n+1}^{g-1} \quad (92)$$

$$\bar{\mathbf{C}}_{n+1} = \mathbf{F}_{n+1}^{veT} \mathbf{F}_{n+1}^{ve} \quad (93)$$

$$\bar{\mathbf{a}}_{n+1} = \mathbf{F}_{n+1}^g \mathbf{a}_0 \quad (94)$$

$$\bar{\mathbf{n}}_{n+1} = \mathbf{F}_{n+1}^g \mathbf{n}_0 \quad (95)$$

$$\alpha_{n+1} = \alpha_n + (h_1 + h_2 \alpha_n) \Delta \lambda_n \quad (96)$$

Compute  $\Delta \mathbf{F}_n^{ve} = \mathbf{F}_{n+1}^{ve} \mathbf{F}_n^{ve-1}$ , update  $\tilde{\mathbf{F}}_{n+1}$ ,  $\hat{\mathbf{F}}_n$  and  $\bar{\mathbf{S}}_{n+1}$  by using the algorithm in Appendix A, then

$$\Delta \lambda_n = \Delta t \frac{\bar{\phi}_{dev}(\bar{\mathbf{S}}_{n+1}, \bar{\mathbf{a}}_{n+1}, \alpha_{n+1})}{\eta} \quad (97)$$

$$\dot{\lambda}_{vol}(t_{n+1}) = \tilde{\zeta}_n \frac{\Delta \lambda_n}{\Delta t} \quad (98)$$

It is noted that the update algorithm involves a nonlinear equation of the unknown variable  $\Delta \lambda_n$ . The Newton-Raphson method is used to solve this nonlinear equation. The calculation of the derivative  $d\bar{\phi}_{dev}/d\Delta \lambda_n (= m\phi^{m-1} d\phi/d\Delta \lambda_n)$  is the key point for applying the Newton-Raphson method, which was discussed in our previous work [51].

### 5.6.2 The elasto-viscoplastic tangent modulus

The spatial total viscoelasto-viscoplastic tangent modulus consistent with the stress update algorithm is given as [53][54 p.294]

$$\mathbf{c}^{\text{viscoelasto-viscoplasticity}} = \mathbf{c} - \frac{(J^{-1}\mathbf{c}:\text{sym}\hat{\mathbf{r}} + \hat{\mathbf{r}} \cdot \boldsymbol{\sigma} + \boldsymbol{\sigma} \cdot \hat{\mathbf{r}}^T) \otimes (\bar{\phi}_\tau : \mathbf{c})}{\eta / \Delta t + (\bar{\phi}_\tau : \mathbf{c}:\text{sym}\hat{\mathbf{r}}) + \bar{\phi}_\alpha} \quad (99)$$

where tensor  $\hat{\mathbf{r}}$  is defined as

$$\hat{\mathbf{r}} = \mathbf{F}_{n+1}^{e-T} \bar{\mathbf{C}}_{n+1} \bar{\mathbf{R}}_n \mathbf{F}_n^g \mathbf{F}_{n+1}^{g-1} \mathbf{F}_{n+1}^{e-1}, \quad (100)$$

tensor  $\bar{\phi}_\tau$  is defined as

$$\bar{\phi}_\tau = \partial \bar{\phi}_{dev} / \partial \boldsymbol{\tau} = \mathbf{F}^{e-T} \text{sym} \bar{\mathbf{R}}^* \mathbf{F}^{e-1}, \quad (101)$$

and function  $\bar{\phi}_\alpha = \partial \bar{\phi}_{dev} / \partial \alpha$  is given in eqn. (84).

## 6 Numerical implementation

Although the motivation for this model is to be able to model the growth of the cells of terrestrial plants, such as the root cells of *Arabidopsis Thaliana*, it is difficult to undertake reliable and accurate experiments on such cells due to their small size. Accordingly, the numerical case studies for the present work relate to *Chara*, which has cells which are several orders of magnitude larger than those of conventional plants. The differences are not just a matter of scale. The cell wall growth of terrestrial plants is believed to be governed by the breaking and reforming of hemicelluloses cross-links, whereas in *Chara* it appears that a similar role is performed by calcium pectate, controlled by the concentration of calcium ions [77]. The presence of calcium ions inhibits bond loosening, while depletion of calcium ions causes bond loosening and permits growth to occur. Although the biochemical details are different from those for terrestrial plant cells, the underlying mechanisms are sufficiently similar that *Chara* has been studied in order to gain an understanding of plant cell behaviour [77]. For this reason, published data on the response of *Chara* to pressure loading [16][66] are used here, and in an earlier study [51], as the basis of a series of case studies.

The applied force technique [8], e.g. loading and unloading by changing the turgor pressure, has been used in the experimental study of cell wall mechanical properties. Different components of deformation have occurred and have been mixed together in an *in vivo* growth process to create a

complex constitutive response that may make the interpretation difficult. Although tremendous experimental data was reported indicating the complexity of mechanical behaviours of cell wall, most of those biology-orientated experiments do not avail for quantitative modelling from the point of view of solid mechanics since they were not designed and reported in a way relevant to constitutive modelling. Proseus and co-workers [16][66][69][75][78] presented a series of novel experimental reports on the growth of internode cells of *Chara coralline* as a system in which turgor pressure, temperature and growth interact with each other. Their experiments were noticeably relevant to constitutive modelling while great attentions were paid to the underlying mechanisms of mechanical regulation of growth. Besides singling out and measuring elastic response, their experimental observations have been widely considered as clear evidence of viscoelastic and viscoplastic behaviours of growing cell wall [7][31]. Nevertheless, numerical modelling has not been reported in the literature to model the observations, until our previous publication [51] was presented.

However, because viscoelasticity was not been taken into account, the coexistence of viscoelastic and viscoplastic responses was not been modelled in our previous work. The numerical implementation of the present model aims to cover those observations in which viscoelastic responses may play an important role and are not negligible. It is noted that viscoelastic responses is observed widely in various plant cell walls [8]. As a phenomenological model based on established experimental observations and widely-accepted hypotheses of general plants, the present constitutive model can be applied to the numerical modelling of other plants if experimental data are available. In Table 2, the methods to estimate the values of parameters in the present model from the available experimental data are presented, which may provide guidance for other experiments to measure the parameters in the model for other plant cell walls.

The geometry of the model is shown in Fig. 6. The *Chara* cell wall can be considered as a closed cylindrical solid shell with length,  $L_0$ , inner radius,  $r_i (= 0.5\text{mm})$ , and thickness,  $\delta (= 10\mu\text{m})$  [79], subjected to inner pressure  $P$ . Microfibrils are aligned transversely in the cell wall. According to the experimental design and observation [16][66] and the theoretical analysis proposed by Boudaoud [31], the effect of tip growth of the cell wall can be ignored when compared to the wall elongation. Thus the model is represented as an open cylindrical wall in the present study. The ends of the cell wall are removed and the turgor pressure applied on the ends is replaced by an equivalent axial stress of value  $P r_i / 2\delta$  applied on the undeformed surface of the two end sections of the open cylindrical wall as shown in Fig. 6.

The constitutive law of the present model is written in a user subroutine (UMAT) in the ABAQUS® FE code. All the numerical case studies are computed by ABAQUS® using a mesh of 600 20-noded 3D quadratic (brick) elements, as shown in Fig. 7. The ratio of thickness to radius,  $\delta / r_i = 0.02$ , indicates that cell wall here is a typical thin-walled structure. In the absence of bending, three quadratic elements along the radial direction can give satisfactory precision on the radial inhomogeneity. Due to the symmetry of both geometry and load and the fact that the stress is independent of the longitudinal coordinate, the FE model studies only one-eighth of an open-ended thin-walled cylinder with a smaller length  $L'_0 = 4\text{mm}$ . Symmetric boundary conditions are imposed on the symmetric boundaries. The elongations of the cell walls with their original lengths are obtained by scaling up from the FE solutions because the geometry and boundary conditions indicate that the stress distribution is longitudinal-axis-independent.

The viscoelastic and irreversible responses of cell walls interplaying with turgor pressure and temperature reported by Proseus *et al.* [66], Proseus *et al.* [69] and Proseus and Boyer [16] are modelled in the case studies. To the authors' knowledge, this is the first time that all responses can be covered by a single model. It is worth emphasising that, although in all of the case studies only the numerical results of longitudinal elongation are reported, our validation is not limited to a uniaxial elongation. The components of the anisotropic growth of cell wall in the radial and transverse

directions automatically agree well with experimental observations because the major qualitative characteristics of cell growth, i.e. plastic inextensibility of microfibrils and stable wall thickness, are obtained as the result of the flow rule implemented in all case studies.

## 6.1 Summary of the model parameters and estimation methods

Unlike traditional engineering materials, the mechanical properties of the living cell walls are regulated by the active biological mechanisms. For example, it has been reported that the yield stress may change according to the change of turgor pressure to maintain a stable growth [24]. Therefore, it is unlikely that a single set of parameters would be found to fit the data obtained from the available range of experiments. The *Chara* cells used in the experiments reported by Proseus *et al.* varied from one case to the other [16][66][69][75][78], so the model parameters may have different values accordingly in the different case studies. However, some parameters, e.g. the overstress sensitivity-exponent and the parameters in the Arrhenius equation of viscosities, take the same values in all the cases.

Table 2 provides a summary of the model parameters used in the FE analysis and methods for parameter estimation. Noting that Young's moduli of wall matrix and microfibrils were the only elastic parameters reported by the experiments. With Young's moduli of wall matrix,  $E$ , obtained, the two parameters  $\kappa$  and  $\mu$  in the hyperelastic response of the cell wall matrix are calculated by the conversion equations,  $\kappa = E/(3(1-2\nu))$  and  $\mu = E/(2(1+\nu))$ , respectively. By implementing the conversion equations in ABAQUS UMAT for neo-Hookean hyperelastic material, the effectiveness of such conversion was justified by the numerical experiment (results not reported here) which indicated that such UMAT yields exactly the same results as ABAQUS Standard Hyperelasticity for any finite strain case studies. Given experimental data, an initial estimation of model parameters can be obtained by using the values and methods provided in Table 2. The initial estimation of some parameters such as Young's modulus and viscosity can be obtained by using the method reported in authors previous work [51] based on the analytical solution of a simplified small strain model. To obtain better fitting to the experimental data, FE simulation is required to optimise the parameter estimation.

It should be noted that the elongation experiments reported by Proseus and co-workers can provide data for a reasonable estimation of parameters of elastic, viscoelastic and viscoplastic responses. Uniaxial tensile tests covering elasticity, creep, relaxation, and hysteresis of the cell wall at growing and non-growing conditions can provide data to estimate the material parameters for the present model. However, as the present model is a fibre-reinforced model, other types of experiments such as indentation [80] may provide data for better estimation of the anisotropic properties.

**Table 2:** Model parameters and estimation

Hyperelasticity	$E$ (Young's modulus of the cell wall matrix)	The value of $E$ ranges from 1.5 to 5.0 GPa for <i>Chara</i> wall matrix (converted from Fig. 8 by Proseus <i>et al.</i> [66] according to the geometry of wall). The range can be estimated more precisely if experimental data for the elastic response is available. The above estimated range of $E$ values coincides with the values used by Niklas [76] and is supported by the finding that the key load-bearing component of the wall matrix, i.e. hemicelluloses cross-links, may have Young's modulus ranging from 8.0 GPa to 10.0 GPa depending on moisture content [81]. The elastic modulus of hemicelluloses also indicates that the
-----------------	---	--

		wall matrix of other plants may have lower Young's modulus, from several MPa to several hundreds MPa, as mentioned by Niklas [76].
	$\nu$ (Poisson's ratio of the cell wall matrix)	$\nu$ is estimated as 0.3 according to the hypothesis that the cell wall is a porous material [78]. Although Poisson's ratio can change under loading conditions, the assumption that the Poisson's ratio of an isotropic biomaterial is constant is valid for many types of materials [76]. The value of 0.3 has been considered to be a reasonable estimation for compressible plant cell walls by many researchers [76][82][83] although some plant cell walls were treated as incompressible materials, i.e. $\nu = 0.5$ [76].
	$\kappa_1, \kappa_2$ (microfibrils elastic parameters)	$\kappa_1 = \mu (= E/(2(1+\nu)))$ , $\kappa_2 = 1.0$ . This is estimated by using Young's modulus of single cellulose microfibrils, 150.0 GPa [4], and assuming the volume fraction of microfibrils to be about 1%-3%.
	$\tilde{\gamma}$ and $\hat{\gamma}$	These values range from 0.0 to 1.0, and are estimated by the fraction of the elastic component in the viscoelastic response during loading and unloading respectively.
Viscoelasticity	$\tilde{\tau}_0$ and $\hat{\tau}_0$	These values range from 5.0 to 30.0 seconds for a growing cell, and about 200 seconds for a mature cell, and are estimated by the characteristic time of relaxation during loading and unloading respectively.
	$Q_{ve}$ (viscoelastic activation energy) and $T_{ve}$	The values of $Q_{ve} = 11.0R$ and $T_{ve} = 0^\circ C$ are estimated by the viscoelastic responses of the cell wall to the same load with different temperatures.
Viscoplasticity (Growth)	$Y_1, Y_2$ (static yield parameters)	These parameters range from 3.5 to 7.0 MPa (converted from turgor pressure threshold from 0.2 to 0.4 MPa [27]). It is noted that, if the reference configuration ( $t = 0$ ) has an unknown history of growth during the time interval $t \in (-\infty, 0]$ , values of $Y_1$ and $Y_2$ actually are the <i>dynamic</i> yield thresholds $(1+h _{t=0})Y_1$ and $(1+h _{t=0})Y_2$ with an unknown $h _{t=0}$ . The dynamic yield thresholds can be estimated by using the method suggested in our previous work [51] if experimental data of growth rates under two different turgor pressures are available. Our FE simulation shows that the dynamic yield thresholds range from 7.0 to 8.0 MPa which are higher than the corresponding static thresholds.
	$\eta_0$ (viscosity)	The value of $\eta_0$ is around several $10^{11} Pa \cdot s$ , estimated from the experimental data of growth (curves of rate of elongation vs time, which were

	reported by Proseus and co-workers [16][66][69]) by using the method suggested in our previous work [51].
$m$ (Overstress sensitivity-exponent)	The value of $m=1.0$ is obtained by using the method of least-squares to fit the original experimental data of <i>Chara</i> cell growth rate, $\dot{L}$ , versus turgor pressure, $P$ ([69], Fig. 13a, temperature=23°C).
$h_1, h_2$ (hardening parameters)	The values of $h_1 \approx 20.6$ and $h_2 \approx 20.0$ are obtained by numerical experiments to fit the experimental data of long-term growth ([16], Fig. 4). For the experimental data of a short-term growth without obvious hardening, $h_1$ can be smaller than 20.6 to obtain better fitting.
$Q$ (growth activation energy) $T_0$ (model parameter)	The values of $Q=50.0R$ and $T_0 = 0^\circ\text{C}$ are estimated by using the method of least-squares to fit the experimental data of the natural logarithm of the normalised growth rate versus $1/T$ ([66], Fig. 4a).
$t_c$ (characteristic time)	The value of $t_c = 10\text{s}$ is estimated according to experimental data ([66], Fig. 2) where a time interval of 10s was short enough to keep natural growth negligible.

## 6.2 Case studies of the cell wall growth

### ***Case study 1: Components of cell elongation: change in length of a cell wall when turgor pressure $P$ is rapidly changed with $P$ pulses***

In this case, the cell solution was injected using a pressure probe to increase  $P$  by 0.04 MPa in 10 seconds.  $P$  was kept at the new level for 10 seconds and then returned to the original level (0.526 MPa) in 10 seconds. This process was repeated twice with two minutes between each pulse as shown in Fig. 8(a). The  $P$  pulse produced both an elastic response and *in vitro* growth as reported by Proseus *et al.* ([66], Fig. 2). Whether the *in vitro* growth is a viscoplastic or viscoelastic response is still an open question [6][9]. One possible interpretation is that viscoplastic response dominates *in vitro* growth and leads to an irreversible expansion (viscoplastic hypothesis). The other interpretation is that the *in vitro* growth is dominated by the retarded elastic response which, given sufficient time, can be shown to be a reversible response (viscoelastic hypothesis). In the present study, the *in vitro* growth reported by Proseus *et al.* can be modelled as behaviour dominated by either the viscoelastic or viscoplastic response. Therefore, the argument about whether the *in vitro* growth is viscoplastic or viscoelastic can be reconciled in the present model. A numerical model which considers the viscoplastic response as the dominant effect was reported in our previous work [51]. Here only the numerical study adopting the viscoelastic hypothesis is presented.

The cell is initially 13 mm long. Since the response of cell wall to the decrease of turgor pressure is dominated by the longitudinal elastic deformation of the wall matrix, Young's modulus of the cell wall matrix is chosen as  $E=3.0$  GPa to fit the elastic shrinkage of cell wall due to the drop of turgor pressure reported by Proseus *et al.* ([66], Fig. 2), and Poisson's ratio is assumed as  $\nu = 0.3$ . The parameters of the microfibrils' elastic response are set as  $\kappa_1 = \mu$  and  $\kappa_2 = 1.0$ . For the viscoelastic response,  $\tilde{\gamma}$  and  $\hat{\gamma}$  are set as 0.28 and 0.0, respectively.  $\tilde{\tau}_0$  and  $\hat{\tau}_0$  are set as 5 seconds and 60

seconds, respectively. For the viscoplastic response, the yield parameters,  $Y_1$  and  $Y_2$ , are set as  $Y_1 = Y_2 = 7.625 \text{ MPa}$ . The viscosity parameter  $\eta_0$  in eqn. (78) is set as  $7.042829 \times 10^{11} \text{ Pa} \cdot \text{s}$ . Hardening parameters are taken as  $h_1 = 61.8$  and  $h_2 = 60.0$ . For the purpose of demonstration, the fitting process to obtain the values of parameters was conducted manually in order to achieve a subjectively good fit; more sophisticated least-squares methods could be employed.

The FE solutions are shown in Fig. 8(b) compared with the experimental data ([66], Fig. 2b). The results indicate that there are three components in the elongation of cell wall: (1) *in vivo* growth, (2) *in vitro* growth, and (3) elastic response.

In Fig. 8(b), Part ① of the elongation is the *in vivo* growth under constant turgor pressure. During this stage,  $\dot{\lambda}_{vol}$  exactly matches  $\dot{\lambda}$  to maintain a constant wall thickness. Part ② of the elongation, which is the *in vitro* growth produced by the  $P$  pulse of pressure, is a mix of the viscoelastic response and irreversible growth. As the characteristic time  $t_c$  is set large enough by comparison with the time interval (30s) of the  $P$  pulse, the change of  $\dot{\lambda}_{vol}$  lags behind the change of  $\dot{\lambda}$  during the *in vitro* growth (result not shown). Finally, Fig. 8(b) shows part ③ of the elongation which is an elastic response since it is assumed that the viscoelastic response during unloading is negligible ( $\gamma^- = 0$ ).

It is noted that neither the elastic model nor the viscous model alone can represent the experimental observation in this case study. The case study indicates that the complex behaviour of the growing cell wall requires constitutive modelling to accommodate various hypotheses. It is interesting that some seemingly contradictory hypotheses, e.g. the viscoplastic hypothesis vs. viscoelastic hypothesis about the *in vitro* growth, can be reconciled in the present constitutive model.

### ***Case study 2: Effects of turgor pressure changes: pressure steps for growing young cells and mature cells***

Case study 1 has shown that a mix of *in vivo* growth and *in vitro* growth occurs under the rapid  $P$  pulses. To study the effect of turgor pressure change on *in vivo* growth, in the reported experiment ([16], Fig. 3a) the  $P$  steps were generated with a pressure probe by removing or injecting cell solution without changing the environment of the cell as shown in Fig. 9a for a young cell. The original turgor pressure is 0.51 MPa at stage ①. The turgor pressure is increased from its original level up to 0.54 MPa at stage ②. After keeping at this level for 22 minutes, the turgor pressure is decreased to its original level at stage ③.

The cell is initially 17 mm long. Young's modulus of the cell wall matrix is chosen as  $E = 2.325 \text{ GPa}$  to fit the elastic shrinkage of the cell wall reported by Proseus and Boyer ([16], Fig. 3b) due to the drop of turgor pressure, and Poisson's ratio is assumed to be  $\nu = 0.3$ . The parameters of the elastic response of microfibrils are set as  $\kappa_1 = \mu$  and  $\kappa_2 = 1.0$ . For the viscoelastic response,  $\tilde{\gamma}$  and  $\hat{\gamma}$  are set as 0.7518 and 0.35, respectively.  $\tilde{\tau}_0$  and  $\hat{\tau}_0$  are set as 31.0 seconds and 541.9 seconds, respectively. For the viscoplastic response, the yield parameters,  $Y_1$  and  $Y_2$ , are set as  $Y_1 = Y_2 = 7.625 \text{ MPa}$ . The viscosity parameter  $\eta_0$  is  $9.048968 \times 10^{11} \text{ Pa} \cdot \text{s}$ . Hardening parameters are taken as  $h_1 = 20.6$  and  $h_2 = 20.0$ .

The FE solutions are shown in Fig. 9(b) compared with the experimental data ([16], Fig. 3b). The main characteristics of the experimental observation are captured by the numerical solution, i.e. (a) instantaneous elastic response and gradual viscoelastic response for the  $P$  steps, (b) change of growth rate at different  $P$  levels.

In contrast to case study 1 in which the  $P$  pulse was short enough to keep the *in vivo* growth almost negligible, in this case study the turgor pressure was kept at the new levels long enough to indicate the relationship between turgor pressure and *in vivo* growth. Corresponding to the changes of turgor pressure, the *in vivo* growth rate increased from stage ① to stage ②, and then resumed the original growth rate at stage ③. Thus the experimental observation indicates that *in vivo* growth rate can be regulated by turgor pressure. This observation is the experimental foundation of the mechanical modelling of cell wall growth. However, we should bear in mind that, in essence, growth is controlled by biological mechanisms, and the turgor pressure is just a passive driving force. As shown in the following study for a mature cell, the change of turgor pressure cannot alter the absence of growth in a mature cell.

FE solutions for a mature cell are presented in Fig. 9(b) and (d). The Young's modulus of the cell wall matrix is chosen as  $E=1.55$  GPa to fit the elastic deformation (shrinkage) when turgor pressure drops ([16], Fig. 3e). The viscoelastic parameters,  $\tilde{\gamma}$  and  $\hat{\gamma}$ , are set as 0.25 and 0.12, respectively. Parameters  $\tilde{\tau}_0$  and  $\hat{\tau}_0$  are set as 2033.2 seconds and 58.1 seconds, respectively. To represent the non-growth behaviour of a mature cell, there are the two options in the present model: either raising the yield threshold or raising the viscosity. The two options, although involving different mechanisms from the point of view of solid mechanics, are capable of simulating the absence of cell wall loosening in a mature cell. Thus a higher yield threshold is set as  $Y_1 = Y_2 = 10\text{MPa}$  for a mature cell but the viscosity is kept the same as for a young cell. The numerical results show that the mature cell responds mainly in a viscoelastic mode.

### *Case study 3: Separating elastic deformation from inelastic deformation*

In the experiments involving turgor pressure change by removal or injection of cell content or water, the growth occurs simultaneously with a stress-induced elastic deformation. The idea of separating the elastic deformation from the inelastic deformation is based on the fact that at lower temperatures, e.g.  $3.1^\circ\text{C}$ , growth vanishes and viscoelastic response is small but the elastic response is the same as at the higher temperature, e.g.  $24^\circ\text{C}$ . Thus by subtracting the deformation at the lower temperature from the total deformation at the higher temperature, the inelastic deformation composed of the viscoelastic response and growth at the higher temperature can be obtained.

In this case study, step changes in turgor pressure  $P$  ( $P$  steps) shown in Fig. 10(a) ([69], Fig. 3a) are applied to cause viscoelastic deformation and change of growth rates. The responses of the cell wall when subjected to  $P$  steps at two different temperatures,  $24^\circ\text{C}$  and  $3.1^\circ\text{C}$ , are studied.

The initial length of the cell is 16 mm. Young's modulus of the cell wall matrix is chosen as  $E=2.3$  GPa to fit the elastic elongation of cell wall due to the increase of turgor pressure at  $3.1^\circ\text{C}$  ([69], Fig. 3c), and Poisson's ratio is assumed as  $\nu = 0.3$ . The parameters of the elastic response of microfibrils are set as  $\kappa_1 = \mu$  and  $\kappa_2 = 1.0$ . The viscoelastic parameters  $\tilde{\gamma}$  and  $\hat{\gamma}$  are set as 0.5 and 0.35, respectively.  $\tilde{\tau}_0$  and  $\hat{\tau}_0$  are set as 12.0 seconds and 108.0 seconds, respectively. For the viscoplastic response, the yield parameters,  $Y_1$  and  $Y_2$ , are set as  $Y_1 = Y_2 = 7.875\text{MPa}$ . The viscosity parameter  $\eta_0$  is  $6.475015 \times 10^{11} \text{Pa} \cdot \text{s}$ . Hardening parameters are taken as  $h_1 = 20.6$  and  $h_2 = 20.0$ .

The FE solutions are shown in Fig. 10(b) and (c) together with the corresponding experimental data ([69], Fig. 3b and 3c) for comparison. The inelastic response which is obtained by subtracting the deformation at  $3.1^\circ\text{C}$  from that at  $24^\circ\text{C}$ , is shown in Fig. 10(d) together with the corresponding experimental data ([69], Fig. 3d). The FE solutions show that the present model can represent the experimental observation of the cell wall growth as a 'turgor pressure-temperature' interaction system.

It is noted that Thomas *et al.* [70] reported a similar experimental observation on the leaf growth rate of cells in the expanding zone of leaves of *Lolium temulentum*. Growth rate of the cells was reduced over a range from 30 $\mu\text{m}/\text{min}$  to zero by reducing the temperature of the expanding zone from 20 to 2 $^{\circ}\text{C}$  while turgor pressure remained constant at 0.5 MPa. This observation can be explained by eqn.(78) which is consistent with the conclusion proposed by Thomas *et al.* [70] that growth reduction by using a low temperature is due to changes in cell wall rheology.

#### ***Case study 4: Combined effects of temperature and turgor pressure***

In order to study the interplays between temperature, turgor pressure and growth in the system, an experiment with both temperature and turgor pressure varying with respect to time was carried out by Proseus *et al.* ([69], Fig. 10a, b and c). To further verify the present model, in this case study the reported combination effects of temperature and turgor pressure is modelled. The histories of turgor pressure and temperature adopted from the experimental data of Proseus *et al.* ([69], Fig. 10a and b) are shown in Fig. 11a and b, respectively.

The initial length of the cell is 16 mm. Young's modulus of the cell wall matrix is chosen as  $E=1.45$  GPa to fit both the elastic shrinkage and elongation of cell wall due to the changes of turgor pressure ([69], Fig. 10b), and Poisson's ratio is assumed as  $\nu = 0.3$ . The parameters of the elastic response of microfibrils are set as  $\kappa_1 = \mu$  and  $\kappa_2 = 1.0$ . The viscoelastic parameters  $\tilde{\gamma}$  and  $\hat{\gamma}$  are set as 0.65 and 0.35, respectively.  $\tilde{\tau}_0$  and  $\hat{\tau}_0$  are set as 10.0 seconds and 100.0 seconds, respectively. The yield parameters,  $Y_1$  and  $Y_2$ , are set as  $Y_1 = Y_2 = 6.25\text{MPa}$ . The viscosity parameter  $\eta_0$  is  $3.181207 \times 10^{11} \text{Pa} \cdot \text{s}$ . Hardening parameters are taken as  $h_1 = 2.0$  and  $h_2 = 20.0$ .

The FE solutions are shown in Fig. 11(c) together with the corresponding experimental data reported by Proseus *et al.* ([69], Fig. 10c). The results indicate that the model can accurately represent the combined effects of temperature and turgor pressure on the cell growth.

## **7 Conclusions**

A fibre-reinforced viscoelasto-viscoplastic model is presented to cover some important characteristics of the expansive growth of the cell walls. The kinematics of multiplicative decompositions of the total and viscoelastic deformation gradients are introduced into the model to define the internal variables of the growth and viscoelastic deformations. The cellulose microfibrils are considered explicitly in the anisotropic model to represent their roles in regulating specific growth directions. Viscoelastic constitutive modelling is proposed to accommodate the typical viscoelastic response of cell walls. By introducing an assumption of decomposition of growth based on experimental observations, a yield function and a flow rule are developed in this work to clarify the mechanical mechanisms of the *in vivo* anisotropic growth of cell wall. The interplays between expansive growth and new material deposition are taken into account by the hardening law and the governing equation of wall thickness, which is a vital step for modelling the sustainable growth. The effect of temperature is also taken into account in the model by using Arrhenius equations for both viscoelastic and viscoplastic viscosities. The model is capable of modelling both the *in vivo* growth of the cell wall dominated by viscoplastic response and the *in vitro* deformation dominated by elastic or viscoelastic responses.

The model is formulated in a finite strain format and a numerical scheme is presented, which is applicable to nonlinear FE analysis. The model is incorporated in a user-subroutine in the ABAQUS<sup>®</sup> FE code, and applied to four case studies reflecting different aspects of *Chara* cell growth. The results show that the model is capable of describing the interplay among growth, turgor pressure and

temperature, as justified by the FE solutions which show a good fitting of the experimental data. As a phenomenological model representing general characteristics of the cell walls, the present constitutive model can be applied to the numerical modelling of other plants provided that experimental data are available.

## Acknowledgement

This work was conducted in the Centre for Plant Integrative Biology, University of Nottingham, U.K., which is jointly funded by the BBSRC/EPSRC (BB/D0196131/1) as part of their Systems Biology Initiative. The authors also gratefully acknowledge the valuable input of Prof. M. Bennett, Dr L. Band and Dr Z. Lin to the literature survey.

## References

1. Refregier G, Pelletier S, Jaillard D, Hofte H (2004) Interaction between wall deposition and cell elongation in dark-grown hypocotyl cells in *Arabidopsis*. *Plant Physiology* 135:959-968
2. Cosgrove DJ (2001) Wall structure and wall loosening. a look backwards and forwards. *Plant Physiology* 125:131-134
3. McCann MC, Wells B, Roberts K (1990) Direct visualization of cross-links in the primary plant cell wall. *Journal of Cell Science* 96:323-334
4. Iwamoto S, Kai W, Isogai A, Iwata T (2009) Elastic modulus of single cellulose microfibrils from tunicate measured by atomic force microscopy. *Biomacromolecules* 10:2571-2576
5. Marga F, Grandbois M, Cosgrove DJ, Baskin TI (2005) Cell wall extension results in the coordinate separation of parallel microfibrils: evidence from scanning electron microscopy and atomic force microscopy. *The Plant Journal* 43:181-190
6. Suslov D, Verbelen J-P (2006) Cellulose orientation determines mechanical anisotropy in onion epidermis cell walls. *J Experimental Botany* 57:2183-2192
7. Dumais J, Shaw SL, Steele CR, Long SR, Ray PM (2006) An anisotropic-viscoplastic model of plant cell morphogenesis by tip growth. *Int J Dev Biol* 50:209-222
8. Cosgrove DJ (1993) Wall extensibility: its nature, measurement and relationship to plant cell growth. *New Phytol* 124:1-23
9. Schopfer P (2006) Biomechanics of plant growth. *American Journal of Botany* 93:1415-1425
10. Cosgrove DJ (1998) Cell Wall Loosening by Expansins. *Plant Physiol.* 118: 333-339.
11. Cosgrove DJ (2000) Loosening of plant cell walls by expansins. *Nature* 407:321-326
12. Cosgrove DJ (2005) Growth of the plant cell wall. *Nat. Rev. Mol. Cell Biol.* 6 (11): 850-861.
13. Choi, D, Cho, H, Lee Y (2006) Expansins: expanding importance in plant growth and development. *Physiologia Plantarum* 126: 511-518.
14. Taiz L (1984) Plant cell expansion: regulation of cell wall mechanical properties. *Annual Review of Plant Physiology* 35:585-657
15. Kutschera U (1990) Cell-wall synthesis and elongation growth in hypocotyls of *Helianthus annuus*. *L Planta* 181:316-323
16. Proseus TE, Boyer JS (2006) Identifying cytoplasmic input to the cell wall of growing *Chara corallina*. *J Experimental Botany* 57:3231-3242
17. Rojas ER, Hotton S, Dumais J (2011) Chemically mediated mechanical expansion of the pollen tube cell wall. *Biophysical Journal* 101:1844-1853
18. Fung YC (1993) *Biomechanics: Mechanical Properties of Living Tissues*. Springer, New York
19. Hohl M, Schopfer P (1992) Physical extensibility of maize coleoptile cell walls: apparent plastic extensibility is due to elastic hysteresis. *Planta* 187:498-504
20. Keckes J, Burgert I, Frühmann K, Müller M, Kölln K, Hamilton M, Burghammer M, Roth SV, Stanzl-Tschegg SE, Fratzl P (2003) Cell-wall recovery after irreversible deformation of wood. *Nature Materials* 2:810-814

21. Lockhart JA (1965) An analysis of irreversible plant cell elongation. *J Theor Biol* 8:264-275
22. Lockhart JA (1965) Cell extension. In Bonner J and Varner JE (eds) *Plant Biochemistry*, Academic Press, New York, p827-849
23. Verbelen J-P., Vissenberg K (2007) Cell expansion: Past, present and perspectives. In Verbelen J-P and Vissenberg K (eds.), *The Expanding Cell*, Springer, Berlin, p1-6
24. Green PB, Erickson RO, Buggy J (1971) Metabolic and physical control of cell elongation rate. *In vivo* studies in *Nitella*. *Plant Physiol* 47:423-430
25. Ray PM, Green PB, Cleland R (1972) Role of turgor in plant cell growth. *Nature* 239:163-164
26. Ortega JKE (1990) Governing equations for plant cell growth. *Physiol Planta* 79:116-121.
27. Cosgrove DJ (1986) Biophysical control of plant cell growth. *Ann Rev Plant Physiol* 37:377-405
28. Geitmann A, Ortega JKE (2009) Mechanics and modelling of plant cell growth. *Trends in Plant Science* 14:467-478
29. Pietruszka M (2009) General proof of the validity of a new tensor equation of plant growth. *J. Theoretical Biology* 256:584-585
30. Veytsman BA, Cosgrove DJ (1998) A model of cell wall expansion based on thermodynamics of polymer networks. *Biophysical Journal* 75:2240-2250
31. Boudaoud A (2003) Growth of walled cells: from shells to vesicles. *Physical Review Letters* 91:018104
32. Bruce DM (2003) Mathematical modelling of the cellular mechanics of plants. *Phil Trans R Soc Lond B* 358 :1437-1444
33. Kerstens S, Decraemer WF, Verbelen J-P (2001) Cell walls at the plant surface behave mechanically like fiber-reinforced composite materials. *Plant Physiology* 127:381-385
34. Hettiaratchi DRP, O'Callaghan JR (1978) Structural mechanics of plant cells. *J Theor Biol* 74:235-257
35. Chaplain MAJ (1993) The strain energy function of an ideal plant cell wall. *J theor. Biol* 163:77-97
36. Dyson RJ, Jensen OE (2010) A fibre-reinforced fluid model of anisotropic plant cell growth. *J Fluid Mechanics* 655:472-503
37. Dyson RJ, Band LR, Jensen OE (2012) A model of crosslink kinetics in the expanding plant cell wall: Yield stress and enzyme action. *Journal of Theoretical Biology* 307 125–136
38. Geitmann A (2010) Mechanical modeling and structural analysis of the primary plant cell wall *Current Opinion in Plant Biology*, 13:693-699
39. Geitmann A (2011) Generating a Cellular Protuberance: Mechanics of Tip Growth. In: Wojtaszek P (ed.), *Mechanical Integration of Plant Cells and Plants*, Springer, Berlin, p.117-132
40. Kha H, Tuble SC, Kalyanasundaram S, Williamson RE (2010) WallGen, Software to Construct Layered Cellulose-Hemicellulose Networks and Predict Their Small Deformation Mechanics. *Plant Physiology*, 152:774-786
41. Goriely A, Tabor M (2003) Biomechanical models of hyphal growth in actinomycetes *Journal of Theoretical Biology* 222:211-218
42. Bernal R, Rojas ER, Dumais J (2007) The mechanics of tip growth morphogenesis: what we have learned from rubber balloons. *Journal of Mechanics of Materials and Structures* 2:1157-1168
43. Hamant O, Heisler MG, Jönsson H, Krupinski P, Uyttewaal M, Bokov P, Corson F, Sahlin P, Boudaoud A, Meyerowitz EM, Couder Y, Traas J (2008) Developmental patterning by mechanical signals in *Arabidopsis*, *Science* 322:1650-1655
44. Kierzkowski D, Nakayama N, Routier-Kierzkowska A-L, Weber A, Bayer E, Schorderet M, Reinhardt D, Kuhlemeier C, Smith RS (2012) Elastic domains regulate growth and organogenesis in the plant shoot apical meristem, *Science*, 335:1096-1099
45. Baskin TI (2005) Anisotropic expansion of the plant cell wall. *Annu Rev Cell Dev Biol* 21: 203-222
46. Epstein M, Maugin GA (2000) Thermomechanics of volumetric growth in uniform bodies. *I J Plasticity* 16:951-978

47. Kuhl E, Steinmann P (2003) Mass- and volume-specific views on thermodynamics for open systems *Proc. R. Soc. Lond. A* 459:2547-2568
48. Guillou A, Ogden RW (2006) Growth in soft biological tissue and residual stress development. In Holzapfel GA and Ogden RW (eds) *Mechanics of Biological Tissue*, Springer-Verlag, Berlin, pp. 47-62
49. Garikipati K, Arruda EM, Grosh K, Narayanan H, Calve S (2004) A continuum treatment of growth in biological tissue the coupling of mass transport and mechanics. *Journal of the Mechanics and Physics of Solids* 52:1595-1625
50. Humphrey JD, Rajagopal KR (2002) A constrained mixture model for growth and remodeling of soft tissues. *Mathematical Models and Methods in Applied Sciences* 12:407-430
51. Huang R, Becker AA, Jones IA (2012) Modelling cell wall growth using a fibre-reinforced hyperelastic-viscoplastic constitutive law. *Journal of the Mechanics and Physics of Solids* 60: 750-783
52. Simo JC, Hughes TJR (1998) *Computational Inelasticity*. Springer, New York
53. Moran B, Ortiz M, Shih CF (1990) Formulation of implicit finite element methods for multiplicative finite deformation plasticity. *International J. for Numerical Methods in Engineering* 29:483-514
54. Belytschko T, Liu WK, Moran B (2001) *Nonlinear Finite Elements for Continua and Structures*. John Wiley & Sons, Chichester
55. Marsden JE, Hughes TJR (1994) *Mathematical Foundation of Elasticity*. Dover, New York.
56. Gasser TC, Ogden RW, Holzapfel GA (2006) Hyperelastic modelling of arterial layers with distributed collagen fibre orientations. *J R Soc Interface* 3:15-35
57. Skalak R (1981) Growth as a finite displacement field. In Carlson DE and Shield RT (eds), *Proceedings off the IUTAM Symposium on Finite Elasticity*, Martinus Nijhoff Publishers, The Hague, p347-355
58. Chuong CJ, Fung YC (1986) Residual stress in arteries. in Schmid-Schonbein, G.W., Woo, SL-Y. and Zweifach, B.W. (Eds.), *Frontiers in Biomechanics*, Springer, New York, p117-129.
59. Chuong CJ, Fung YC (1986) On residual stresses in arteries. *J Biomech Eng* 108:189-192
60. Fung YC (1990) *Biomechanics: Motion, Flow, Stress, and Growth*. Springer, New York
61. Rodriguez EK, Hoger A, McCulloch A (1994) Stress-dependent finite growth in soft elastic tissue. *J Biomech* 27:455-467
62. Lee EH (1969) Elastic-plastic deformation at finite strain. *J Appl Mech ASME* 36:1-6
63. Gasser TC, Forsell C (2011) The numerical implementation of invariant-based viscoelastic formulations at finite strains. An anisotropic model for the passive myocardium, *Comput. Methods Appl. Mech. Engrg.*, 200:3637-3645
64. Humphrey JD, Rajagopal KR (2003) A constrained mixture model for arterial adaptations to a sustained step change in blood flow. *Biomech Model Mechanobiol* 2:109-126
65. Maugin GA (1999) *The Thermomechanics of Nonlinear Irreversible Behaviours*. World Scientific Publishing Ltd., Singapore
66. Proseus TE, Ortega JKE, Boyer JS (1999) Separating growth from elastic deformation during cell enlargement. *Plant Physiology* 119:775-784
67. Reese S, Govindjee S, (1998) A theory of finite viscoelasticity and numerical aspects. *Int. J. Solids Structures*, 35:3455-3482
68. Spencer AJM (2001) A theory of viscoplasticity for fabric-reinforced composites. *Journal of the Mechanics and Physics of Solids* 49:2667-2687
69. Proseus TE, Zhu G-L., Boyer JS (2000) Turgor, temperature and the growth of plant cells using *Chara corallina* as a model system. *Journal of Experimental Botany* 51:1481-1494
70. Thomas A, Tomos AD, Stoddart JL, Thomas H, Pollock CJ (1989) Cell expansion rate, temperature and turgor pressure in growing leaves of *Lolium temulentum* L. *New Phytologist*, 112:1-5
71. Mandel J (1971) *Plasticité Classique et Viscoplasticité (CISM Lecture Notes, Udine, Italy)*. Springer-Verlag, Vienna
72. Lubliner J (1990) *Plasticity Theory*. Macmillan, New York.
73. Maugin GA (2011) *Configurational Forces: Thermo-Mechanics, Physics, Mathematics and*

- Numerics. CRC Press, Boca Raton
74. Epstein M, Maugin GA (1996) On the geometrical structure of anelasticity. *Acta Mechanica* 115:119-131
  75. Proseus TE, Boyer JS (2007) Tension required for pectate chemistry to control growth in *Chara corallina*. *J Experimental Botany* 58:4283-4292
  76. Niklas KJ (1992) *Plant Biomechanics: An Engineering Approach to Plant Form and Function*. University of Chicago Press, Chicago
  77. Boyer, JS (2009) Cell wall biosynthesis and the molecular mechanism of plant enlargement. *Functional Plant Biology*, 36, 383–394
  78. Proseus TE, Boyer JS (2005) Turgor pressure moves polysaccharides into growing cell walls of *Chara corallina*. *Annals of Botany* 95:967-979
  79. Toole GA, Gunning PA, Parker ML, Smith AC, Waldron KW (2001) Fracture mechanics of the cell wall of *Chara corallina*. *Planta* 212:606-611
  80. Milani P, Gholamirad M, Traas J, Arnéodo A, Boudaoud A, Argoul F, Hamant O (2011) In vivo analysis of local wall stiffness at the shoot apical meristem in *Arabidopsis* using atomic force microscopy. *Plant J.* 67:1116-1123
  81. Cousins WJ (1978) Young's modulus of hemicelluloses as related to moisture content. *Wood Science and Technology*, 12:161-167
  82. Wang CX, Wang L, Thomas CR (2004) Modelling the mechanical properties of single suspension-cultured tomato cells. *Annals of Botany* 93: 443-453
  83. Wei C, Lintilhac PM, Tanguay JJ (2001) An insight into cell elasticity and load-bearing ability: Measurement and theory. *Plant Physiology*, 126:1129-1138

## Appendix A: The update algorithm of $\bar{\mathbf{S}}$ and $\bar{\mathbf{C}}^v$

The update criterion (11) for the configuration  $\tilde{\mathbf{B}}_t$  is implemented as follows

$$\tilde{\mathbf{F}}_{n+1} = \Delta\tilde{\mathbf{F}}_n \tilde{\mathbf{F}}_n, \quad \hat{\mathbf{F}}_{n+1} = \Delta\hat{\mathbf{F}}_n \hat{\mathbf{F}}_n \quad (\text{A1})$$

where the increments  $\Delta\tilde{\mathbf{F}}_n$  and  $\Delta\hat{\mathbf{F}}_n$  are defined as follows

$$\begin{cases} \text{if } \text{tr}\mathbf{L}_n^{ve} < 0 & \Delta\tilde{\mathbf{F}}_n = \mathbf{I}, & \Delta\hat{\mathbf{F}}_n = \tilde{\mathbf{F}}_n^{-1} \Delta\mathbf{F}_n^{ve} \tilde{\mathbf{F}}_n \\ \text{if } \text{tr}\mathbf{L}_n^{ve} \geq 0 & \Delta\tilde{\mathbf{F}}_n = \Delta\mathbf{F}_n^{ve}, & \Delta\hat{\mathbf{F}}_n = \mathbf{I} \end{cases} \quad (\text{A2})$$

in which the velocity gradient  $\mathbf{L}_n^{ve}$  is computed from  $\Delta\mathbf{F}_n^{ve}$  by using the relation

$$\Delta\mathbf{F}_n^{ve} = (\mathbf{I} + \mathbf{L}_n^{ve} \Delta t_n). \quad (\text{A3})$$

The update of the algorithmic internal variables  $\tilde{\mathbf{H}}_{n+1}$  and  $\hat{\mathbf{H}}_{n+1}$  is obtained by using the middle rule [52] as follows

$$\tilde{\mathbf{H}}_{n+1} = \tilde{\mathbf{H}}_n + \exp(-\Delta t_n / 2\tilde{\tau}) \tilde{\mathbf{S}}_{n+1}^\circ, \quad (\text{A4})$$

$$\hat{\mathbf{H}}_{n+1} = \hat{\mathbf{H}}_n + \exp(-\Delta t_n / 2\hat{\tau}) \hat{\mathbf{S}}_{n+1}^\circ \quad (\text{A5})$$

where  $\tilde{\mathbf{H}}_n$  and  $\hat{\mathbf{H}}_n$  are defined as

$$\tilde{\mathbf{H}}_n = \exp(-\Delta t_n / \tilde{\tau}) \tilde{\mathbf{H}}_n - \exp(-\Delta t_n / 2\tilde{\tau}) \tilde{\mathbf{S}}_n^\circ, \quad (\text{A6})$$

$$\widehat{\mathbf{H}}_n = \exp(-\Delta t_n/\bar{\tau})\widehat{\mathbf{H}}_n - \exp(-\Delta t_n/2\bar{\tau})\widehat{\mathbf{S}}_{n+1}^\circ. \quad (\text{A7})$$

In order to obtain expressions of  $\bar{\mathbf{S}}$  and  $\bar{\mathbf{C}}^v$ , specified functions  $W^\circ$  and  $\tilde{W}^\circ$  in eqn.(38) and (39) are set in the similar form as the deviatoric part of the free energy of wall matrix in eqn.(31) as follows

$$W^\circ(\hat{\mathbf{C}}) = \frac{1}{2}\mu(\text{tr}\hat{\mathbf{C}} - 3), \quad (\text{A8})$$

$$W^\circ(\hat{\mathbf{C}}) = \frac{1}{2}\mu(\text{tr}\hat{\mathbf{C}} - 3) = \frac{1}{2}\mu(\hat{\mathbf{C}}:\hat{\mathbf{b}}^{-1} - 3) = \tilde{W}^\circ(\hat{\mathbf{C}}, \hat{\mathbf{b}}). \quad (\text{A9})$$

Thus the stress tensors  $\tilde{\mathbf{S}}_{n+1}^\circ$  and  $\widehat{\mathbf{S}}_{n+1}^\circ$  in eqn.(A4) and (A5) is obtained by using eqns.(38) and (39) as

$$\tilde{\mathbf{S}}_{n+1}^\circ = \widehat{\mathbf{F}}_n^{-1}\tilde{\mathbf{S}}_{n+1}^\circ\widehat{\mathbf{F}}_n^{-T} \text{ in which } \tilde{\mathbf{S}}_{n+1}^\circ = \mu\bar{J}_{n+1}^{-2/3}\text{DEV}_{n+1}^+[\mathbf{I}], \quad (\text{A10})$$

$$\widehat{\mathbf{S}}_{n+1}^\circ = \mu\bar{J}_{n+1}^{-2/3}\text{DEV}_{n+1}\left[\hat{\mathbf{b}}_{n+1}^{-1}\right] \quad (\text{A11})$$

where the deviatoric operators are defined as

$$\text{DEV}_{n+1}^+[(\square)] = (\square) - \frac{1}{3}(\tilde{\mathbf{C}}_{n+1} : (\square))\tilde{\mathbf{C}}_{n+1}^{-1}, \quad (\text{A12})$$

$$\text{DEV}_{n+1}[(\square)] = (\square) - \frac{1}{3}(\bar{\mathbf{C}}_{n+1} : (\square))\bar{\mathbf{C}}_{n+1}^{-1}. \quad (\text{A13})$$

Substituting eqns.(A4),(A5),(A10),(A11) into eqn.(45) yields

$$\begin{aligned} \bar{\mathbf{S}}_{n+1} &= \bar{\mathbf{S}}_{n+1}^e \\ &- \bar{J}_{n+1}^{-2/3}\tilde{\mathbf{g}}_n^*\text{DEV}_{n+1}[\tilde{\mathbf{S}}_{n+1}^\circ] + \bar{J}_{n+1}^{-2/3}\tilde{\gamma}\text{DEV}_{n+1}[\tilde{\mathbf{H}}_n] \\ &- \bar{J}_{n+1}^{-2/3}\hat{\mathbf{g}}_n^*\widehat{\mathbf{S}}_{n+1}^\circ + \bar{J}_{n+1}^{-2/3}\hat{\gamma}\text{DEV}_{n+1}[\widehat{\mathbf{H}}_n] \end{aligned} \quad (\text{A14})$$

where the two functions  $\tilde{\mathbf{g}}_n^*$  and  $\hat{\mathbf{g}}_n^*$  are defined respectively as

$$\tilde{\mathbf{g}}_n^* = 1 - \exp(-\Delta t_n/2\bar{\tau}), \quad \hat{\mathbf{g}}_n^* = 1 - \exp(-\Delta t_n/2\bar{\tau}). \quad (\text{A15})$$

By using eqn.(A14), eqn.(24) indicates that the viscoelastic components of tangent modulus is

$$\begin{aligned} \bar{\mathbf{C}}_{n+1}^v &= -\bar{J}_{n+1}^{-2/3}\tilde{\mathbf{g}}_n^*\text{DEV}_{n+1}\left[\frac{\partial\tilde{\mathbf{S}}_{n+1}^\circ}{\partial\bar{\mathbf{C}}}\right] - \bar{J}_{n+1}^{-2/3}\hat{\mathbf{g}}_n^*\frac{\partial\widehat{\mathbf{S}}_{n+1}^\circ}{\partial\bar{\mathbf{C}}} \\ &+ \frac{\partial\{\bar{J}_{n+1}^{-2/3}\text{DEV}_{n+1}\}}{\partial\bar{\mathbf{C}}}\left[-\tilde{\mathbf{g}}_n^*\tilde{\mathbf{S}}_{n+1}^\circ + \tilde{\gamma}\tilde{\mathbf{H}}_n + \hat{\gamma}\widehat{\mathbf{H}}_n\right] \end{aligned} \quad (\text{A16})$$

where two operators,  $\text{DEV}[(\square)]$  and  $\partial\{\bar{J}^{-2/3}\text{DEV}\}/\partial\bar{\mathbf{C}}[(\square)]$ , are defined, respectively, as

$$\text{DEV}[(\square)] = (\square) - \frac{1}{3}\bar{\mathbf{C}}^{-1} \otimes (\bar{\mathbf{C}} : (\square)), \quad (\text{A17})$$

$$\begin{aligned} \frac{\partial\{\bar{J}^{-2/3}\text{DEV}\}}{\partial\bar{\mathbf{C}}}[(\square)] &= \bar{J}^{-2/3}\left\{-\frac{2}{3}\text{DEV}[(\square)] \otimes \bar{\mathbf{C}}^{-1} - \frac{2}{3}\bar{\mathbf{C}}^{-1} \otimes \text{DEV}[(\square)]\right. \\ &\left.+ \frac{2}{3}((\square) : \bar{\mathbf{C}})\left[\mathbf{I}_{\bar{\mathbf{C}}^{-1}} - \frac{1}{3}\bar{\mathbf{C}}^{-1} \otimes \bar{\mathbf{C}}^{-1}\right]\right\}. \end{aligned} \quad (\text{A18})$$

The remaining work is to compute two tensors  $\partial\widehat{\mathbf{S}}_{n+1}/\partial\bar{\mathbf{C}}$  and  $\partial\widetilde{\mathbf{S}}_{n+1}/\partial\bar{\mathbf{C}}$  in eqn.(A16).

By using eqns.(A11) and (A18),  $\partial\widehat{\mathbf{S}}_{n+1}/\partial\bar{\mathbf{C}}$  is obtained straightforward as

$$\frac{\partial\widehat{\mathbf{S}}_{n+1}}{\partial\bar{\mathbf{C}}} = \mu \frac{\partial\left\{\bar{J}_{n+1}^{-2/3}\text{DEV}_{n+1}\right\}}{\partial\bar{\mathbf{C}}}\left[\widehat{\mathbf{b}}_{n+1}^{-1}\right]. \quad (\text{A19})$$

On the other hand, by using the criterion (A2) (if  $\text{tr}\mathbf{L}^e \geq 0$ ),  $\partial\widetilde{\mathbf{S}}_{n+1}/\partial\bar{\mathbf{C}}$  is computed by the chain rule as follows

$$\frac{\partial\widetilde{\mathbf{S}}_{n+1}}{\partial\bar{\mathbf{C}}} = \frac{\partial\widetilde{\mathbf{S}}_{n+1}}{\partial\widetilde{\mathbf{C}}}\left(\frac{\partial\widetilde{\mathbf{C}}}{\partial\bar{\mathbf{C}}}\right)_n \quad (\text{A20})$$

where tensor  $\partial\widetilde{\mathbf{S}}_{n+1}/\partial\widetilde{\mathbf{C}}$  is expressed as

$$\left[\frac{\partial\widetilde{\mathbf{S}}_{n+1}}{\partial\widetilde{\mathbf{C}}}\right]_{IJKL} = \left[\widehat{\mathbf{F}}_n^{-1}\right]_{IS}\left[\widehat{\mathbf{F}}_n^{-1}\right]_{JT}\left[\frac{\partial\widetilde{\mathbf{S}}_{n+1}}{\partial\widetilde{\mathbf{C}}}\right]_{STKL} \quad (\text{A21})$$

in which by using eqn.(A10) we have

$$\begin{aligned} \frac{\partial\widetilde{\mathbf{S}}_{n+1}}{\partial\widetilde{\mathbf{C}}} &= \frac{2}{3}\mu\widetilde{J}_{n+1}^{-2/3}\left\{\left(\text{tr}\widetilde{\mathbf{C}}_{n+1}\right)\left[\mathbf{I}_{\widetilde{\mathbf{C}}_{n+1}^{-1}} - \frac{1}{3}\widetilde{\mathbf{C}}_{n+1}^{-1} \otimes \widetilde{\mathbf{C}}_{n+1}^{-1}\right]\right. \\ &\quad \left.- \left[\widetilde{\mathbf{C}}_{n+1}^{-1} \otimes \text{DEV}_{n+1}^+[\mathbf{I}] + \text{DEV}_{n+1}^+[\mathbf{I}] \otimes \widetilde{\mathbf{C}}_{n+1}^{-1}\right]\right\}. \end{aligned} \quad (\text{A22})$$

The other unknown tensor in eqn.(A20),  $\partial\widetilde{\mathbf{C}}/\partial\bar{\mathbf{C}}$ , is deduced as follows. It can be shown that (if  $\text{tr}\mathbf{L}^e \geq 0$ )

$$\widetilde{\mathbf{C}}_{n+1} - \widetilde{\mathbf{C}}_n = \widehat{\mathbf{F}}_n^{-T}\left(\bar{\mathbf{C}}_{n+1} - \bar{\mathbf{C}}_n\right)\widehat{\mathbf{F}}_n^{-1}. \quad (\text{A23})$$

By using eqn.(A23), two one-parameter families of right Cauchy-Green tensors are constructed in the forms of

$$\bar{\mathbf{C}}_\varepsilon = \bar{\mathbf{C}} + \varepsilon\mathbf{H}_n, \quad (\text{A24})$$

$$\widetilde{\mathbf{C}}_\varepsilon = \widetilde{\mathbf{C}} + \varepsilon\widehat{\mathbf{F}}_n^{-T}\mathbf{H}_n\widehat{\mathbf{F}}_n^{-1} \quad (\text{A25})$$

where  $\varepsilon$  is a scalar parameter, tensor  $\mathbf{H}_n$  is defined as

$$\mathbf{H}_n = \bar{\mathbf{C}}_{n+1} - \bar{\mathbf{C}}_n. \quad (\text{A26})$$

The derivative of  $\widetilde{\mathbf{C}}_\varepsilon$  with respect to  $\varepsilon$  is computed from eqn.(A25) as

$$\left.\frac{\partial\widetilde{\mathbf{C}}_\varepsilon}{\partial\varepsilon}\right|_{\varepsilon=0} = \widehat{\mathbf{F}}_n^{-T}\mathbf{H}_n\widehat{\mathbf{F}}_n^{-1}. \quad (\text{A27})$$

The definitions (A24) and (A25) indicate that

$$\left.\frac{\partial\widetilde{\mathbf{C}}_\varepsilon}{\partial\varepsilon}\right|_{\varepsilon=0} = \frac{\partial\widetilde{\mathbf{C}}}{\partial\bar{\mathbf{C}}}\left.\frac{\partial\bar{\mathbf{C}}_\varepsilon}{\partial\varepsilon}\right|_{\varepsilon=0} = \frac{\partial\widetilde{\mathbf{C}}}{\partial\bar{\mathbf{C}}}\mathbf{H}_n. \quad (\text{A28})$$

Therefore, eqns. (A27) and (A28) yield the expression of  $\partial\tilde{\mathbf{C}}/\partial\bar{\mathbf{C}}$  as follows

$$\left[ \left( \frac{\partial\tilde{\mathbf{C}}}{\partial\bar{\mathbf{C}}} \right)_n \right]_{IJKL} = \left[ \hat{\mathbf{F}}_n^{-1} \right]_{KI} \left[ \hat{\mathbf{F}}_n^{-1} \right]_{LJ}. \quad (\text{A29})$$

Once tensors  $\partial\tilde{\mathbf{S}}_{n+1}^\circ/\partial\tilde{\mathbf{C}}$  and  $\partial\tilde{\mathbf{C}}/\partial\bar{\mathbf{C}}$  are obtained by eqns.(A21) and (A29) respectively, eqn.(A20) yields the expression of  $\partial\tilde{\mathbf{S}}_{n+1}^\circ/\partial\bar{\mathbf{C}}$ . Then the expression of  $\bar{\mathbf{C}}^v$  is obtained by substituting eqns.(A17-A20) into eqn.(A16).

## Appendix B: The derivative of function $\phi$

Let  $(\square)$  be an entity standing for tensor, vector or scalar. By taking the derivative of eqn. (67) with respect to  $(\square)$  we obtain

$$\frac{\partial\theta}{\partial(\square)} = \mathfrak{g}_1 \frac{\partial\bar{J}_1}{\partial(\square)} + \mathfrak{g}_2 \frac{\partial\bar{J}_2}{\partial(\square)} + \mathfrak{g}_h \frac{\partial h}{\partial(\square)} \quad (\text{B1})$$

where

$$\mathfrak{g}_1 = Y_1^2 (\theta - Y_2^2)^2 / \mathfrak{g}_D, \quad \mathfrak{g}_2 = Y_2^2 (\theta - Y_1^2)^2 / \mathfrak{g}_D, \quad \mathfrak{g}_h = -(\theta - Y_1^2)^2 (\theta - Y_2^2)^2 / \mathfrak{g}_D \quad (\text{B2})$$

in which

$$\mathfrak{g}_D = 2 \left\{ (1+h)(\theta - Y_1^2)(\theta - Y_2^2)(2\theta - Y_1^2 - Y_2^2) - \bar{J}_1 Y_1^2 (\theta - Y_2^2) - \bar{J}_2 Y_2^2 (\theta - Y_1^2) \right\}. \quad (\text{B3})$$

Using the chain rule and substituting eqn. (B1) into the derivative of the distance function  $\phi$  with respect to  $(\square)$  yields

$$\frac{\partial\phi}{\partial(\square)} = \left( \frac{\partial\phi}{\partial\bar{J}_1} + \mathfrak{g}_1 \frac{\partial\phi}{\partial\theta} \right) \frac{\partial\bar{J}_1}{\partial(\square)} + \left( \frac{\partial\phi}{\partial\bar{J}_2} + \mathfrak{g}_2 \frac{\partial\phi}{\partial\theta} \right) \frac{\partial\bar{J}_2}{\partial(\square)} + \mathfrak{g}_h \frac{\partial\phi}{\partial\theta} \frac{\partial h}{\partial(\square)} \quad (\text{B4})$$

in which

$$\begin{aligned} \frac{\partial\phi}{\partial\bar{J}_1} &= \frac{\theta^2}{2\phi(Y_1^2 - \theta)^2}, \quad \frac{\partial\phi}{\partial\bar{J}_2} = \frac{\theta^2}{2\phi(Y_2^2 - \theta)^2}, \\ \frac{\partial\phi}{\partial\theta} &= \frac{\phi}{\theta} + \frac{\theta^2}{\phi} \left( \frac{\bar{J}_1}{(Y_1^2 - \theta)^3} + \frac{\bar{J}_2}{(Y_2^2 - \theta)^3} \right). \end{aligned} \quad (\text{B5})$$

## Figure captions

Fig. 1 Distribution of cellulose microfibrils and the cross-links in cell walls.

Fig. 2 Responses of the growing cell wall to the changes of turgor pressure with rapid elastic, viscoelastic, and viscoplastic components.

Fig. 3 The different geometric configurations and their relationships

Fig. 4 Growth mechanisms of cell wall (a) Isochoric expansive growth without irreversible microfibrils extension driven by Spencer's deviatoric stress where covalent bonds and hydrogen bonds are broken. (b) Volumetric growth without irreversible microfibrils extension driven by the stress regulating the deformation of the new wall polymers.

Fig. 5 The closest point projection in the space of stress invariants.

Fig. 6 Geometry of the computational model.

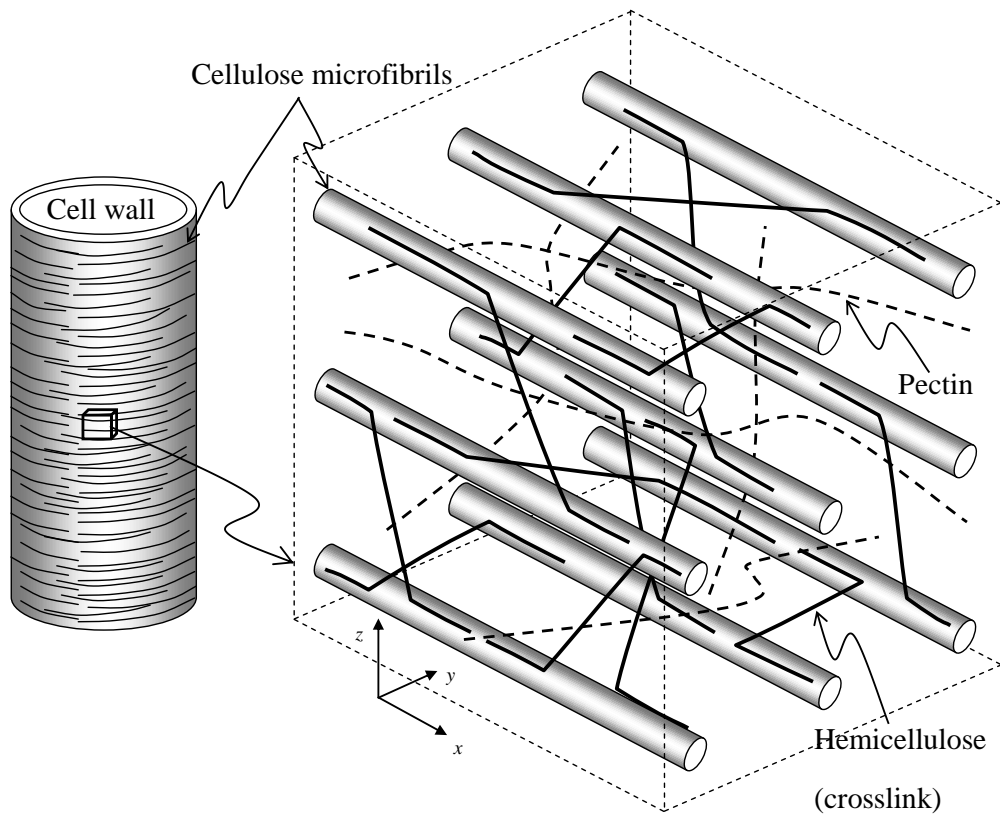
Fig. 7 FE mesh representing one-eighth of the cylinder

Fig. 8 Effects of  $P$  pulses: (a)  $P$  pulses superimposed on normal turgor pressure. (b) Cell elongation.

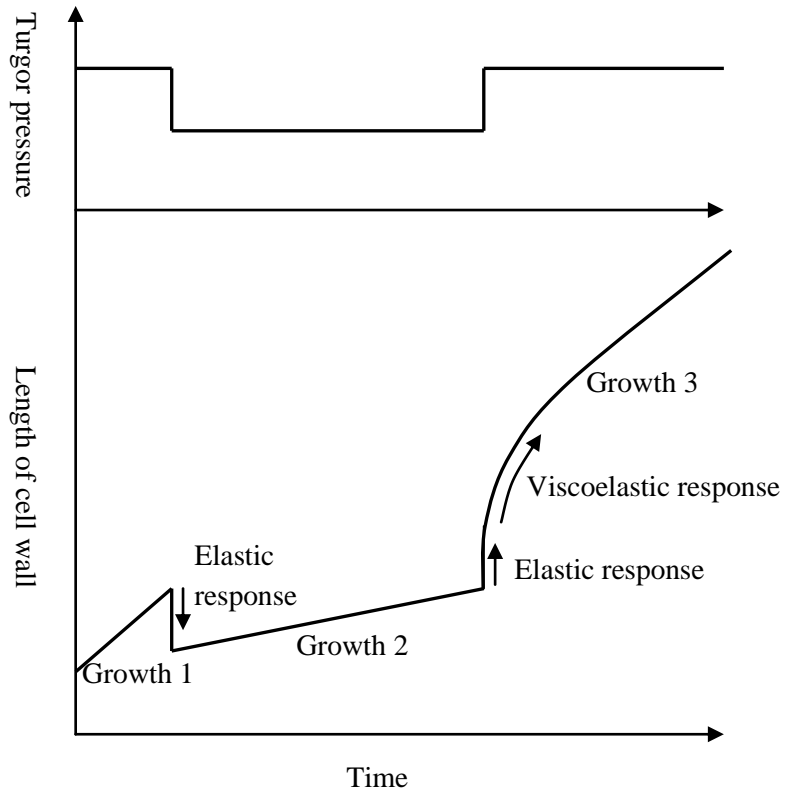
Fig. 9 The effect of turgor pressure change on the deformation of young and mature cells. (a) turgor pressure vs time for a young cell, (b) length change vs time for a young cell, (c) turgor pressure vs time for a mature cell, (d) length change vs time for a mature cell.

Fig. 10 Growth interaction with turgor pressure and temperature. (a) turgor pressure vs time, (b) length change vs time at 24°C, (c) length change vs time at 3.1°C, (d) inelastic length change vs time.

Fig. 11 The combination effect of the temperature and turgor pressure changes on the growth of young cell. (a) temperature vs time, (b) turgor pressure vs time, (c) length change vs time.



**Fig. 1** Distribution of cellulose microfibrils and the cross-links in cell walls



**Fig. 2** Responses of the growing cell wall to the changes of turgor pressure with rapid elastic, viscoelastic, and viscoplastic components.

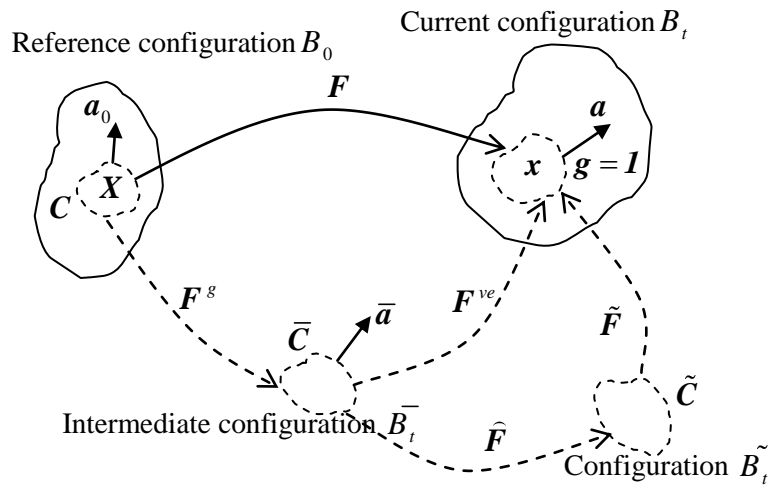


**Fig. 3** Different geometric configurations and their relationship.

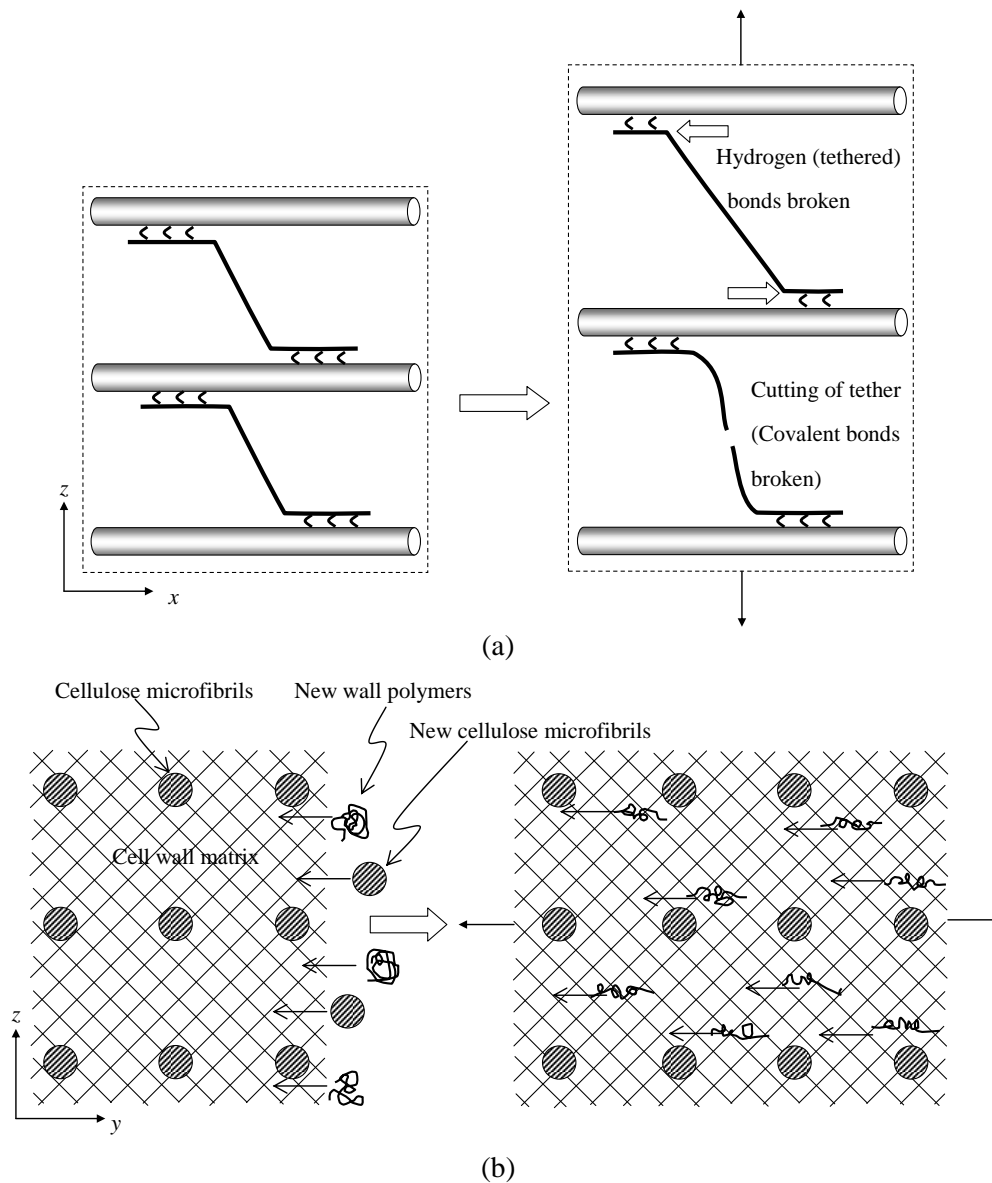


**Fig. 4** Growth mechanisms of cell wall (a) Isochoric expansive growth without irreversible microfibrils extension driven by Spencer's deviatoric stress where covalent bonds and hydrogen bonds are broken. (b) Volumetric growth without irreversible microfibrils extension driven by the stress regulating the deformation of the new wall polymers.

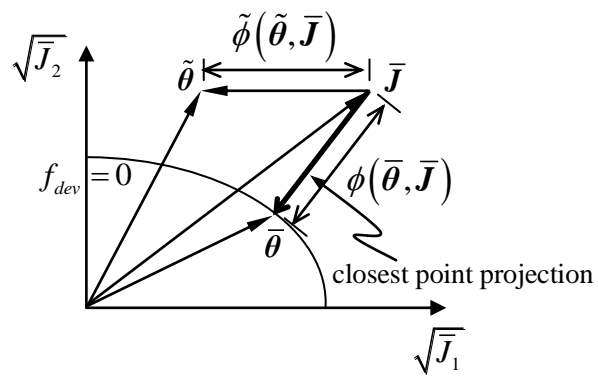


**Fig. 5** The closest point projection in the space of stress invariants.

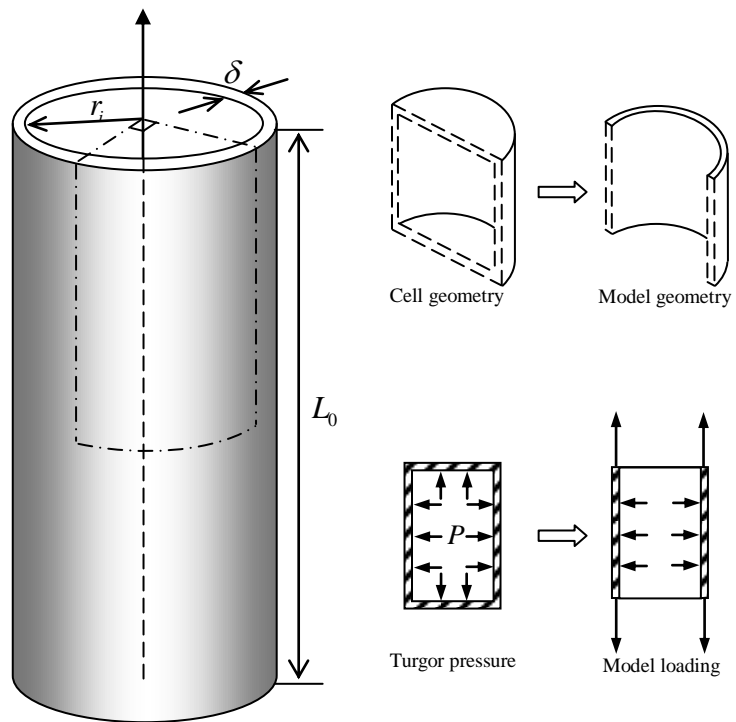


**Fig. 6** Geometry of the computational model

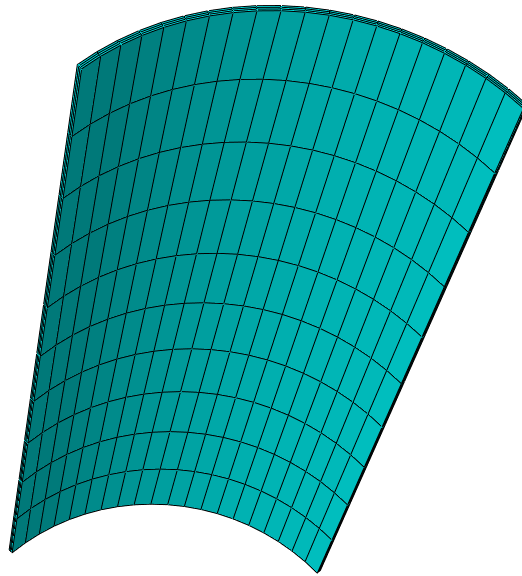
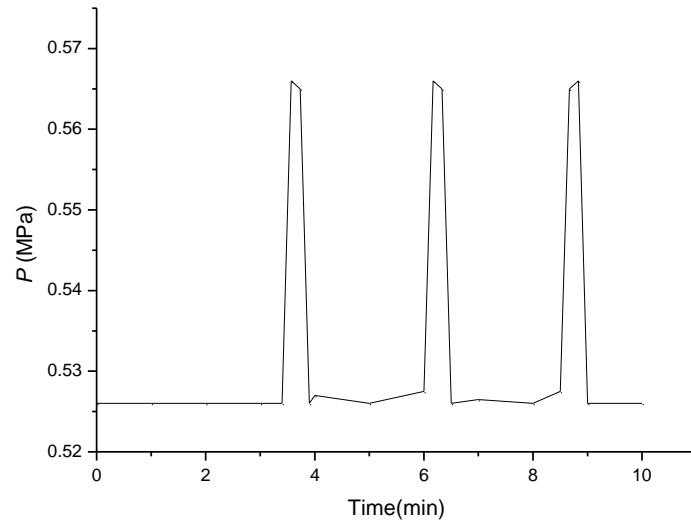
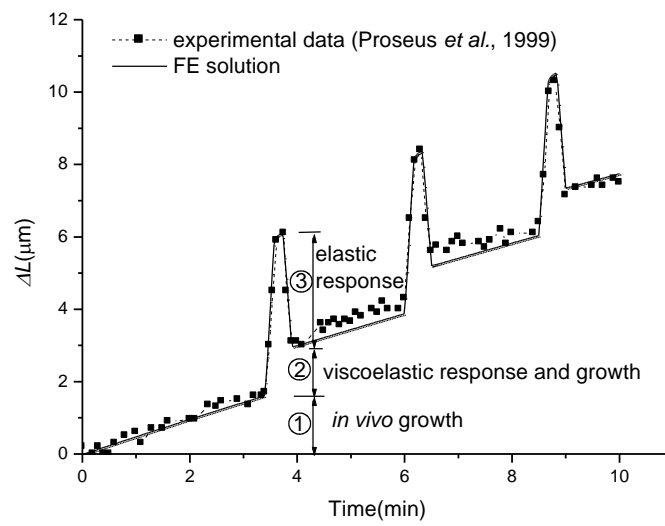


**Fig. 7** FE mesh representing one-eighth of the cylinder

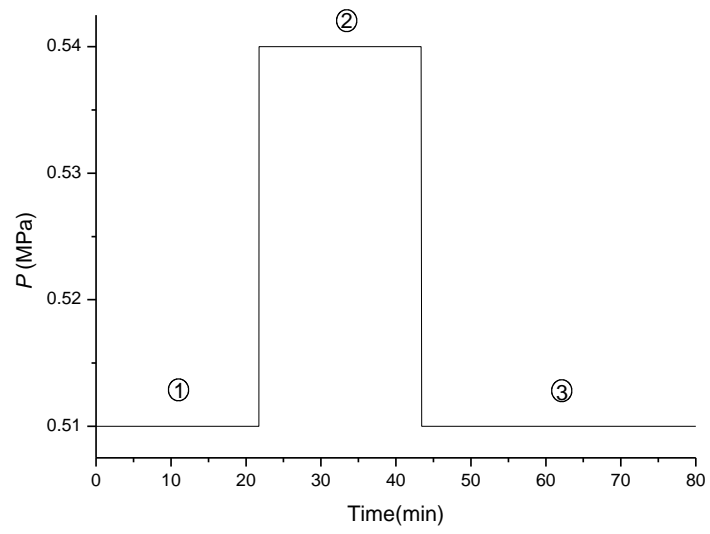


(a)

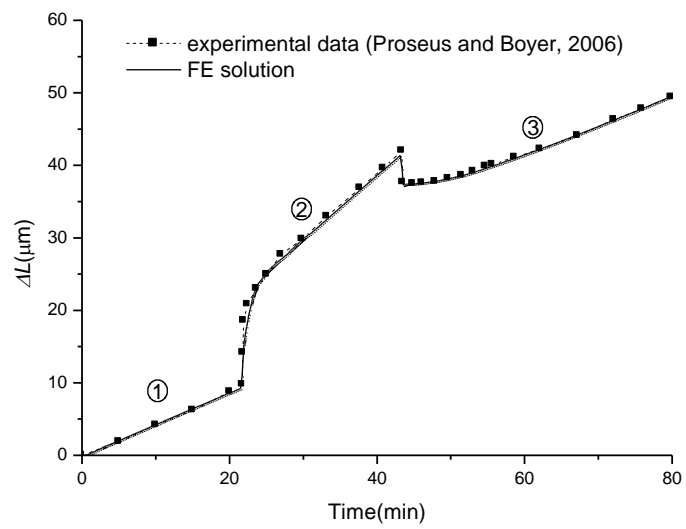


(b)

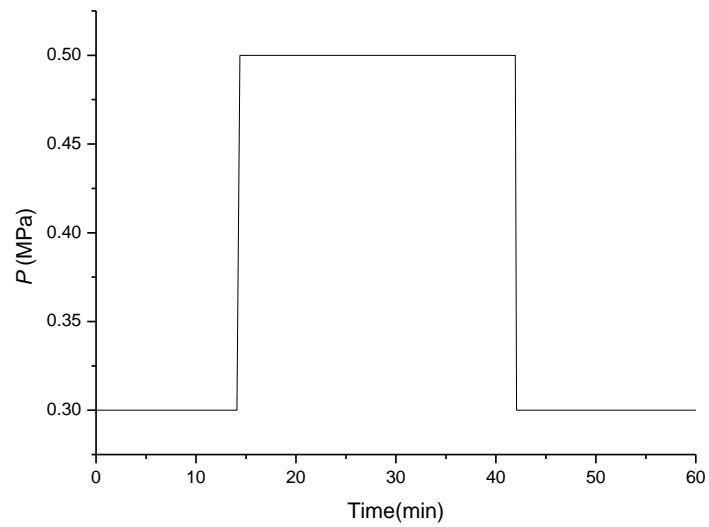
**Fig. 8** Effects of  $P$  pulses: (a)  $P$  pulses superimposed on normal turgor pressure. (b) Cell elongation.



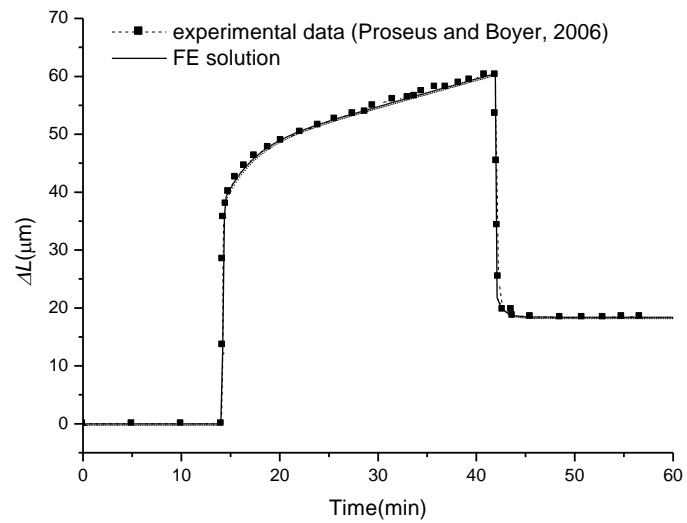
(a)



(b)

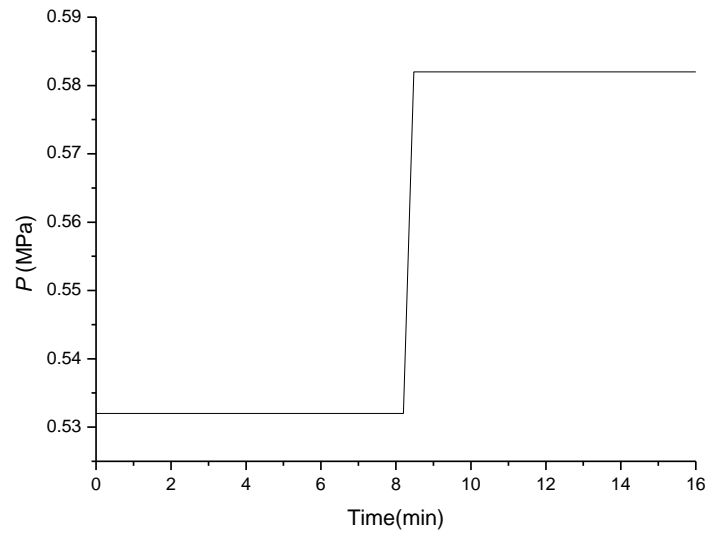


(c)

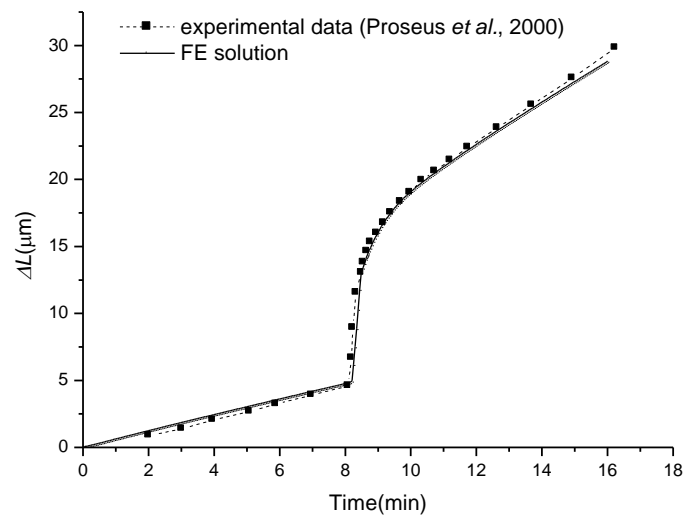


(d)

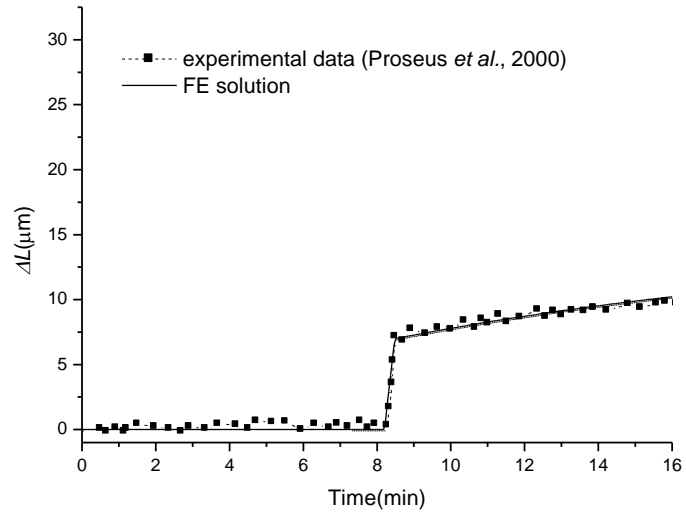
**Fig. 9** The effect of turgor pressure change on the deformation of young and mature cells. (a) turgor pressure vs time for a young cell, (b) length change vs time for a young cell, (c) turgor pressure vs time for a mature cell, (d) length change vs time for a mature cell.



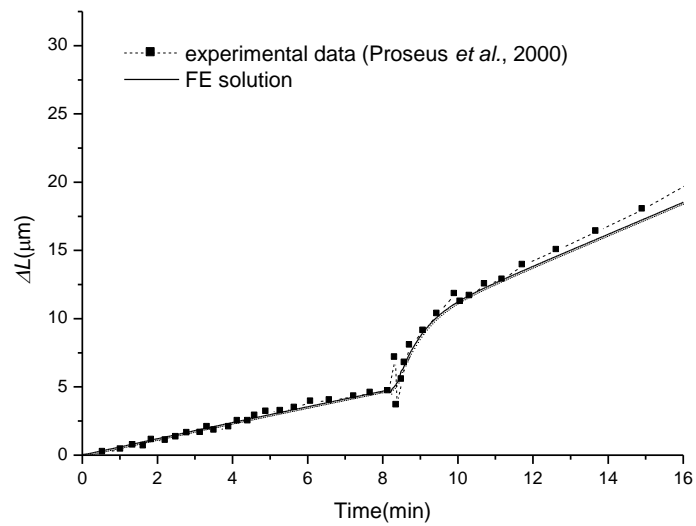
(a)



(b)

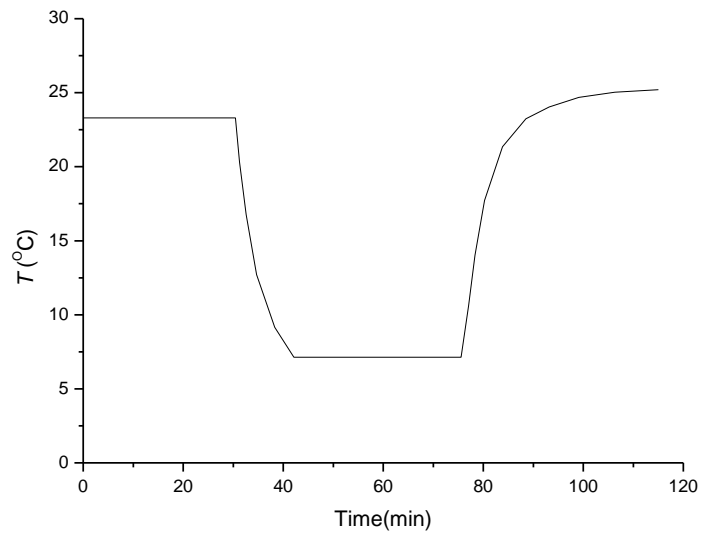


(c)

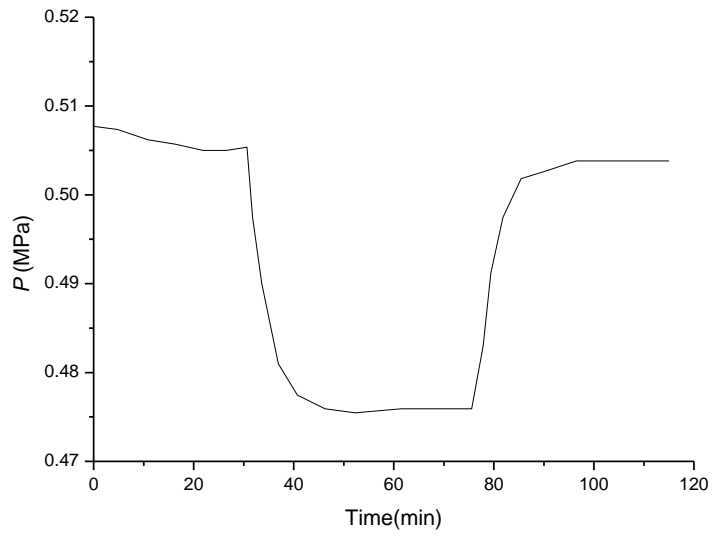


(d)

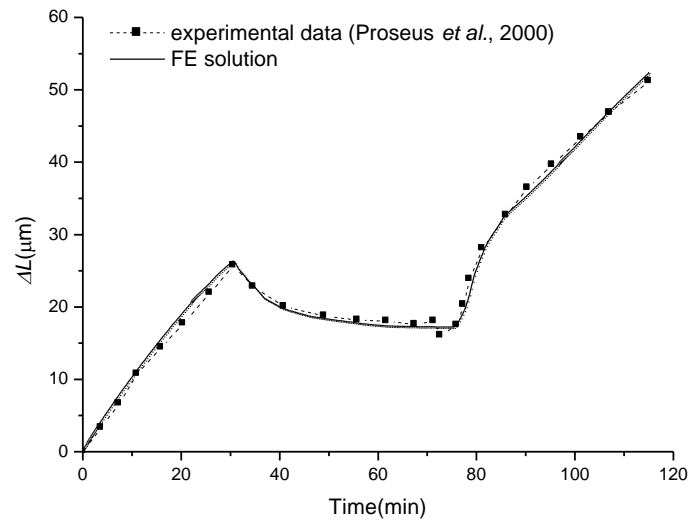
**Fig. 10** Growth interaction with turgor pressure and temperature. (a) turgor pressure vs time, (b) length change vs time at  $24^\circ\text{C}$ , (c) length change vs time at  $3.1^\circ\text{C}$ , (d) inelastic length change vs time.



(a)



(b)



(c)

**Fig. 11** The combination effect of the temperature and turgor pressure changes on the growth of young cell. (a) temperature vs time, (b) turgor pressure vs time, (c) length change vs time.